Optical Design Group

MWI CONCEPTUAL DESIGN REVIEW

Simon Thibault
Mélanie Leclerc
Jean-François Lavigne
Michel Poirier
René Doyon

Revision No.	**Author & Date**	**Approval & Date**	**Description**
Revision 1	Simon Thibault 2004-09-30	Simon Thibault 2004-09-30	Creation
Revision 2	Simon Thibault 2004-10-20	Simon Thibault 2004-10-19	Mid-term document

TABLE OF CONTENTS

1 PURPOSE

The MWI Conceptual Design describes the MWI Imager for the EXAOC project (INO 030165).

2 APPLICABLE DOCUMENTS

Document ID	**Source**	**Title**
mwi_concept_specs_v1.0.pdf	EXAOC strawman design	Multi-Wavelength Imager Concept & Specifications (Strawman Design)

3 DEFINITIONS AND ACRONYMS

CFHT	Canada France Hawaii Telescope
EXAO	Extreme Adaptative Optics
EXAOC	Extreme Adaptative Optics Coronagraph
F/#	F number
FFOV	Full Field of view
FOC	Fore Optic Converter
FOV	Field of View
GSAOI	Gemini South Adaptive Optic Imager
IFU	Integral Field Unit
INO	Institut National d'Optique
IR	Infrared
MCDA	Multicolor detector assembly
MFOV	Medium Field of view
MW	Multi-Wavelength
MWI	Multi-Wavelength Imager
OAP	Off-axis parabola
PSF	Point Spread Function
RSAA	Research School of Astronomy and Astrophysics
Trident	
UdeM	Université de Montréal
WIRCAM	Wide field Infrared Camera

4 OVERVIEW

This document summarizes the contents of the conceptual design of the Multi-wavelength imager of the EXAOC project (GEMINI).

4.1 Design Concept and Priority

The MWI produces 4 discrete narrow (R~30-50) band images simultaneously on the same detector enabling speckle suppression through PSF subtraction and/or the spectral “deconvolution”.

A crucial functionality of the MWI is to suppress speckle noise with the highest possible efficiency ideally down to the photon-noise limit. A key requirement for the MWI is to avoid the effect of non-common path optics, which has been shown to be the main limiting factor of the MWI TRIDENT camera.

One important figure of merit for the MWI and the IFU is the noise attenuation factor τ defined as $\Delta N/N$ where N is the original PSF noise in the coronagraphic image and ΔN is the residual noise left after PSF subtraction. For example, the TRIDENT camera on CFHT achieved a τ~0.3/0.1 without/with reference star calibration. The MWI concept described here should enable τ less than 0.01 over a full FOV. The design presented here is a slightly different (more flexible) implementation of the multicolor detector assembly (MCDA) concept stated in the original proposal.

4.2 Technical Implementation

The INO and University of Montreal (UdeM) will develop the MWI by re-using the many of the designs already developed for the CFHT WIRCAM by UdeM/INO and GSAOI by RSAA. MWI will be mounted in an original cryostat but the instrument will use the same cryogenic mounting scheme and general simple architecture than those imagers. For commodity, mechanism control system hardware and temperature control system hardware can also be duplicated from GSAOI. The instrument sequencer, components controller and engineering interface software developed for GSAOI will also be re-used for MWI with minimum modifications. This safer approach adopted by INO and UdeM in the development of the MWI will help to cut down both schedule and budget.

The MWI imager detector controller software will be probably an evolution of the similar code written for GSAOI HAWAII-2 detector.

4.3 Systems Design

The MWI system is shown in Figure 1 (excluding the fore optic converter). The cryostat includes the fore optic converter, the lenslet array, the collimator, the MW-splitter, the filters, the re-imager and the detector.

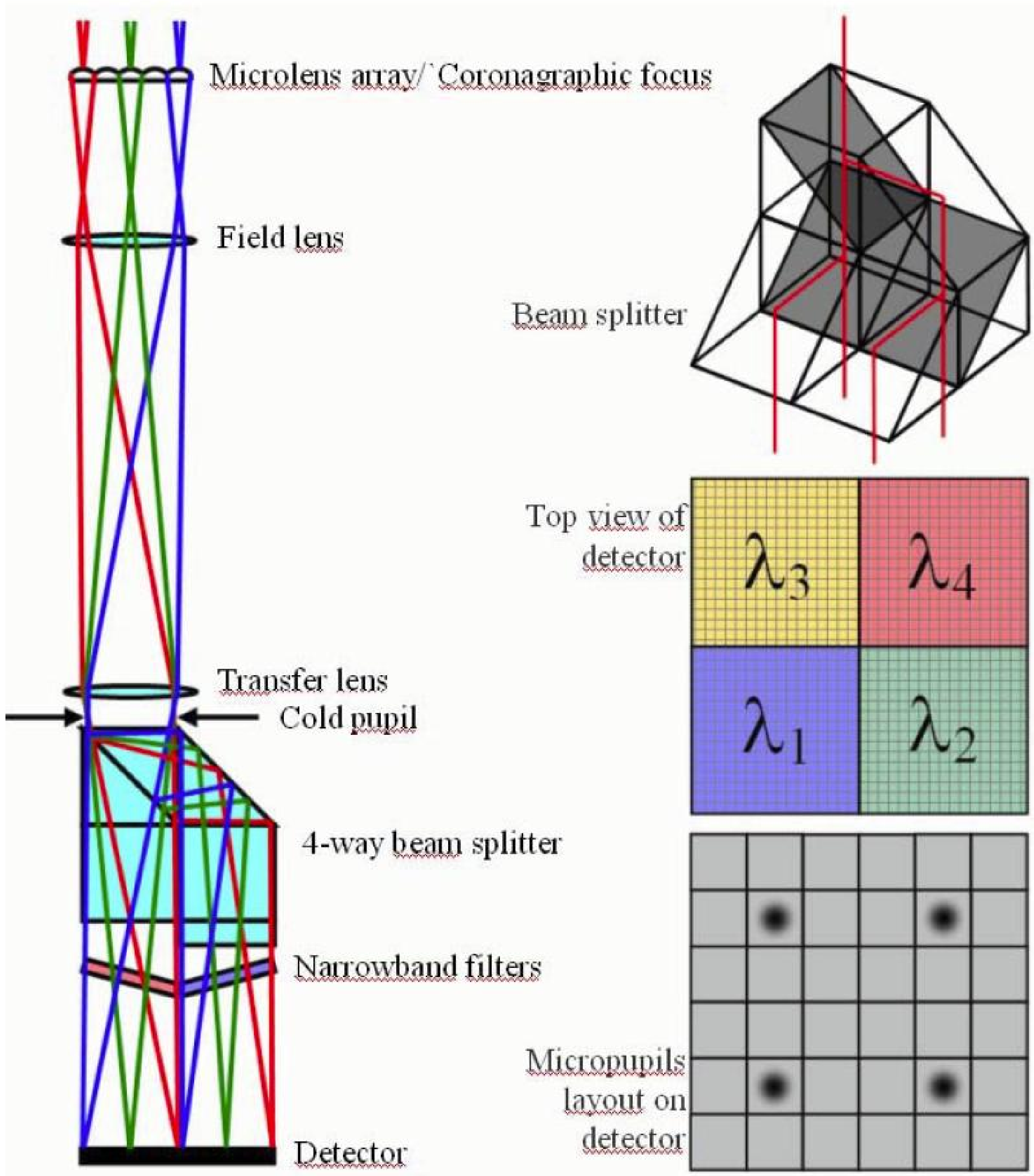

Figure 1:

Figure 1 - MWI baseline optical design

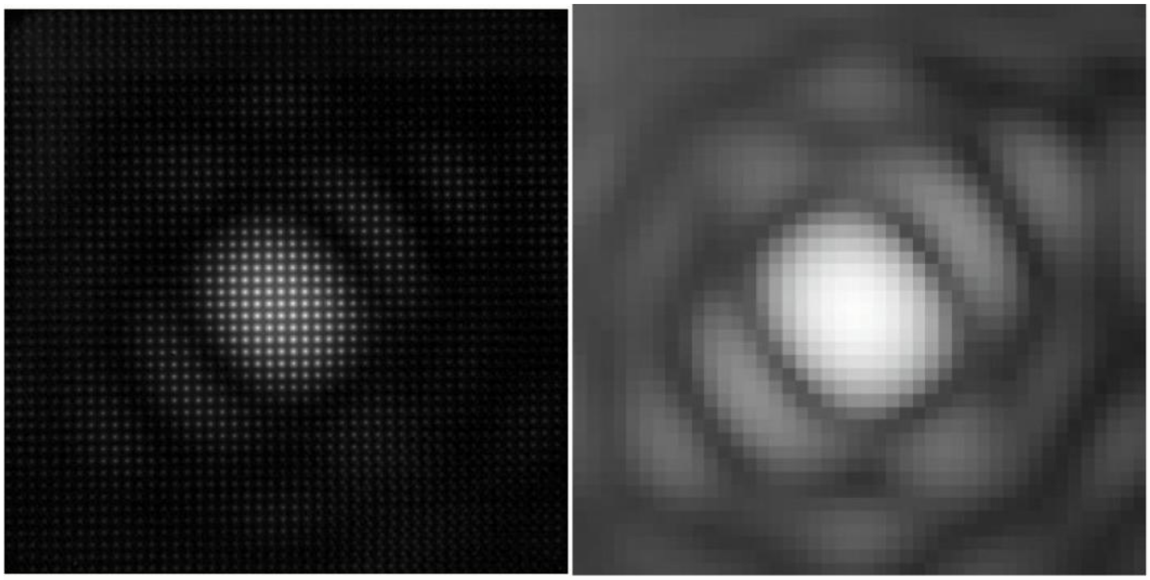

Figure 2:

Figure 2 - Laboratory PSF dissected with a micro-lens array and its reconstruction.

4.4 Optical Design

4.4.1 Concept

A 4-wavelengths MWI concept is sketched in Figure 1 (fore optic converter no shown). The output image of the coronagraph is first dissected by a lenslet array producing an array of micro-pupils. The input focal ratio is such that there is at least 2 micro-lenses per λ/D, each micro-lens having a pitch of ~3 detector pixels. The micro-pupils are then re-imaged through a 4-way beam splitter combined with narrow-band filters to yield 4 PSFs images each spanning one quadrant on an IR detector. The PSF is reconstructed by integrating the signal of each micro-pupil (see Fig. 2) over a 2x2, 3x3 pixel box or a circular aperture. Non-common aberrations are still present in this design but they affect only the shape of individual micro-pupil PSFs, the integrated signal being hardly affected. One important implementation of this design is that there is no contamination from one wavelength to another (wavelength crosstalk).

4.4.2 Fore optic converter

The output of the coronagraph will be a 15 mm collimated beam (from an F/64 off axis parabola). The fore optic converter (FOC) includes the cryostat window, the cold pupil (15 mm) and an off axis parabola (OAP) focusing element that produce an F/90 image plane.

The baseline FOC design is minimal. The FOC should be compact and should deliver an excellent science image plane. This ensures that FOC will not overly degrade the high Strehl ratio achieved by EXAOC optics.

Features of the design:

- The FOC will have an excellent chromatic correction by using reflective optics.
- The cryostat window will be located in a collimated beam so that optical thickness does not cause defocus.
- Polish quality glass off axis parabola will be required. SORL has a high experience on such optical component. However, the cost can be important.

4.4.3 Multi-Wavelength Imager

The baseline MWI imager is reproduced in Figure 3 (unfolded path design). It is a refractive/reflective system consisting of a fused silica lenslet array in the science focal plane produced by the FOC. A collimator triplet is used to collimate the light into the MW-splitter. The collimator uses BaF2 and SF6 glasses that produces a 15 mm diameter pupil image in collimated light in the MW-splitter. The MW-splitter baseline design is to use immersed dichroics (see sketch in Figure 1) to separate all 4 beams with the maximum throughput. It is reasonable to expect throughput in excess of 70% narrow-band filters included. A non-cemented doublet camera using combination of glasses such as ZnSe, SF6 and BaF2 is used for each wavelength channel to re-image the focal plane into the imager detector. A filter is located in collimated space ahead of the doublet camera.

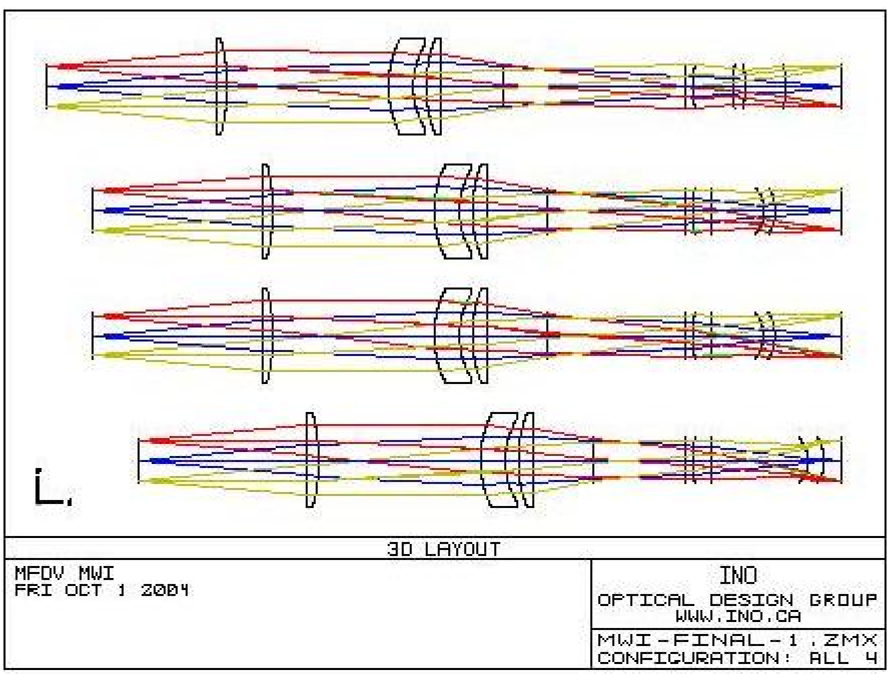

Figure 3

Figure 3 - Unfolded optical layout of the baseline optics showing the MWI parts.

Features of the design:

- 1 to 1 imaging relay that minimizes the optical distortion.
- The location of the MW-splitter in collimated space so that the different optical thickness of each MW-splitter channel do not cause major defocus and aberration problem.
- Compact design that minimizes the overall length.
- Standard glass lenses are used with well known cryogenic refractive indices. Procurement of such glasses will not be a problem.

The potential drawbacks of the design are:

- The MW-splitter using fused silica immersive dichroics is a challenging optical element. Cryogenic multi-elements assemblies have been done in the past, such as polarization cube splitter. However, the MW-splitter may be difficult to procure. Custom assembly should be required. Behavior at cryogenic temperature of such assembly remains problematic and the risk mitigation plan will address this problem. The effect of fabrication errors on the MWI performance will be discussed later.

4.5 Mechanical Design

TBD

4.6 Detector Control Systems

TBD

4.7 Instrument Control System

TBD

4.8 Control Software

TBD

4.9 Summary

5 SYSTEM DESIGN

5.1 Introduction

MWI is a complex instrument comprises various optical components, hardware and software that must work together. It is a part of the EXAOC instrument that will be installed on the Gemini Telescope, and therefore must interface to the Gemini environment.

The manner in which the MWI system interacts with the EXAOC system is described in the following sections.

5.2 MWI Interfaces

The main mechanical sub-systems are the imager detector assembly, the cryocooler, cold work plate (temperature sensor) and pressure gauge.

Control of these subsystems will be performed by an overall control system software, which is defined into the EXAOC system design. However a separate control path exists for the MWI. Software commands originating from the EXAOC Control System are received by the MWI Temperature Control System (MWI-TCS) and by the Detector Controller (MWI-DC). The MWI-TCS drives the cryocoolers, controls the temperature of the imager detector and cold work plate, and monitors the cryostat vacuum pressure. It also controls and monitors various temperature sensors, to perform cool down and warm up functions.

5.3 Environmental Heat Load

The MWI design meets the EXAOC environmental heat load requirement budget. The maximum load that can be conducted into the instrument body is XXW and the maximum acceptable heat load that can be converted into the dome is XXW by the MWI sub-system. The heat generated by the cryocoolers is excluded from this budget.

5.4 Mass Budget

The MWI design meets the EXAOC mass budget, which meets the instrument mass requirement of 2000 Kg. The mass budget for the MWI is presented in Table 1.

Table 1 : MWI Mass Budget

Item	Mass [kg]	Source
Science Camera Interface Plate		
Main Frame		
Cryostat Vacuum Jacket		
MWI (including components)		
Detector Controllers		
Thermal Enclosure		
Detector power supplies		
ICS Controllers		
Cabling		
Miscellaneous		

5.5 Center of Gravity Budget

The MWI design meets the EXAOC center of gravity requirements; weights ballast can be used to get proper center of gravity.

5.6 Instrument Volume

The MWI design meets the EXAOC instrument volume allocation requirements.

5.7 Optical Image Quality Budget

The system image quality budget is divided into two main sub-systems (FOC and MWI). The FOC wavefront errors must be less than 50 nm. The MWI wavefront errors must have Strehl ratio larger the 0.7. The FOC requirement is driven by the quality of the science image plane. The MWI requirement is driven by the energy lost within each lenslet sub-aperture active area. The optical image quality budget is presented in the section TBD

5.8 Throughput Budget

The MWI design meets the requirement of the system throughput, excluding the coronagraph. The throughput budget is presented in the section TBD

5.9 Emissivity Budget

The MWI design meets the requirement of an effective instrument emissivity of < 1% at wavelength > 2μm and an instrument photon background less than one half of the detector dark current.

5.10 Mechanical Flexure Performance

MWI will use the EXAOC guide system to provide tracking and correction. The mechanical flexure performance of the MWI will be within a TBD pixels requirement. The image translation due to mechanical flexure should be monitored during the calibration process. The close proximity of MWI images by using the same detector will eliminate differential translation between images.

5.11 Thermal Enclosure Space Allocation

TBD

5.12 Electrical Power Budget

TBD

5.13 Handling Equipment

TBD

5.14 Calibration Requirements

TBC

5.15 Risk Analysis

A summary of the major risks associated with the development of the MWI is presented in Table 2. An impact on the scientific performance and a risk level have been assigned to each risk items. A Risk Mitigation Plan is also presented in order to address the risk impact or the risk priority.

Table 2 : MWI Risk Mitigation Plan

Item	Description	Science Impact	Risk Level	Priority	Mitigation Plan
1	Science				
1.1					
2	Optical				
2.1	MWI-Splitter				
2.1.1	Dichroic design	H	M	1	Comparative study between immersive design and standard dichroic design will be done (advantages and drawbacks). Develop design variants using dichroic plane parallel plates. Evaluate the thin film design requirements for both dichroic and bandpass filters.
2.1.2	MW-Splitter Assembly	L	L	2	Perform cryogenic assembly on dummy samples. If this fails, adopt a design variant that uses standard dichroic filter plate. INO experience in telecom industry will help.
2.1.3	Dichroic cost	L	M	1	Dichroic supplier must be identified early in the design phase. INO coating department will help us to design and prepare the dichroic requirements properly.
2.1.4	Ghost	M	L	1	Ghost analysis will be done using non-sequential ray tracing and/or ASAP software. INO experience in stray light

					analysis using ASAP will be useful.
2.2	Throughput	H	M	3	Special AR coating for limited waveband can have very high performances. Lens coatings will be obtained from and validated by INO thin film department.
2.3	Lens mounting	M	M	2	Appropriate lens mounting tolerances will be allowed and mounts will be carefully checked before lenses are installed. Mounting technique will be tested on a dummy assembly (point 2.1.2)
3	Mechanical				
3.1					
3.2					
4	Software				
4.1					
4.2					
5	Detector				

6 OPTICAL DESIGN

6.1 Introduction

A 4-wavelengths MWI concept is sketched in Figure 1 (fore optic converter not shown). The output image of the coronagraph is first dissected by a lenslet array producing an array of micro-pupils. The input focal ratio is such that there is at least 2 micro-lens per λ/D, each micro-lens having a pitch of ~3 detector pixels. The micro-pupils are then re-imaged through a 4-ways beam splitter combined with narrow-band filters to yield 4 PSFs images each spanning one quadrant on an IR detector. The PSF is reconstructed by integrating the signal of each micro-pupil (see Fig. 2) over a 2x2, 3x3 pixel box or a circular aperture. Non common aberrations are still present in this design but they affect only the shape of individual micro-pupil PSFs, the integrated signal being hardly affected. One important implementation of this design is that there is a minimum contamination from one wavelength to another (wavelength crosstalk).

6.2 Top level requirements

This section describes the absolute minimum requirements that the strawman must demonstrate to be scientifically viable as the main scientific instrument for the EXAO system.

• **Detector:** Hawaii-2RG 2040x2040, 18 μm pixels

• **Microlens array:** square shape, 54 µm pitch (= 3 detector pixels assuming unit magnification), f/5.6 output corresponding to λf/D~9 µm or half a detector pixel.
• **Input focal ratio:** f/90
• **FOV**: 5.3"x5.3"
• **Spectral resolution:** ~50
• **Wavelengths:** 1.52, 1.58, 1.64 and 1.70 µm

The possibility to use a microlens array with a 72 µm pitch so that four detector pixels cover its area will also be studied. The input focal ratio (FOC) would then be f/120 to keep the same sampling in the focal plane. This setting will be referred to as the 4x4 pixels case while the previous one will be referred to as the 3x3 pixels case. From an optical design point of view, the FOC and the lenslet array will be different. The relay imager will stay the same. However, the FOV will be smaller by the F/# ratio.

6.3 Requirements of the MW-Splitter

The MW-splitter should separate the beam into four wavebands as in Table 3 below.

Channel	CWL (µm)	FWHM (µm)
1	1.70	~ 0.04µm
2	1.64	
3	1.58	
4	1.52	

Table 3 – Wavelengths

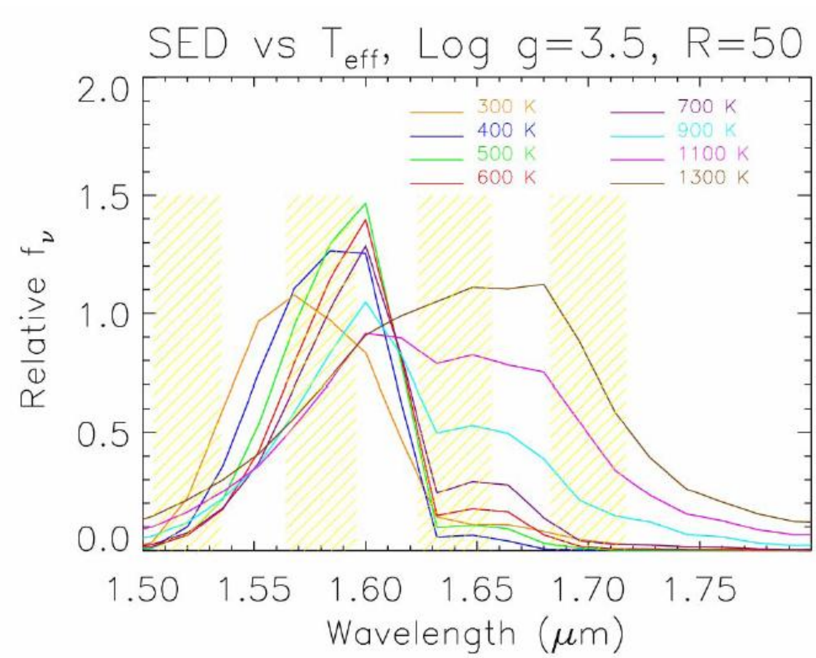

Figure 4 - Theoretical H-band spectra of free-floating exoplanets. The hatched yellow regions correspond to the 4 bandpass (FWHM) of the MWI.

The detector is already chosen and so we have to re-image the micro-pupils as four images at different wavebands, on the four quadrants of this detector.

6.4 MWI Design constraints

A major constraint in the design is a space constraint. The beam must be separated into four beams by the MW-splitter, and the object plane at the lenslet array is re-imaged on each of the four quadrants of the detector. The detector has the following specifications:

Hawaii-2RG
2040 X 2040 Pixels, 18 μm/Pixel

thus, a detector of 18.360 mm half width. Each of the four quadrants will then be of 9.180 mm half width. This dimension will constrain the design and will limit the size of the MW-splitter cube and of each channel exit lens.

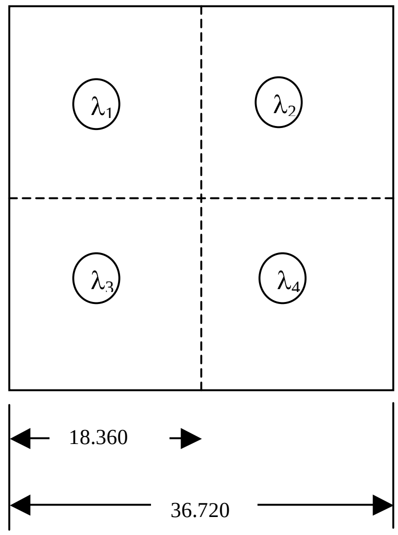

Figure 5 – Detector size

Each exit channel of the MW-splitter cube should not be wider than each detector quadrant, or 18.360 mm.

Each channel will have a different path length in the beam splitter cube:

Channel 1 (λ=1.70μm):	4 × cube width
Channel 3 (λ=1.58μm):	3 × cube width
Channel 2 (λ=1.64μm):	3 × cube width
Channel 4 (λ=1.52μm):	2 × cube width

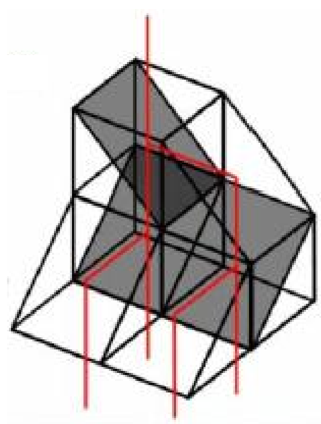

Figure 6 – MW-splitter cube

We chose to associate the longer wavelengths with the longer Optical Path Lengths (OPL) to minimize as best we could the Optical Path Difference (OPD) and to have more similar optical components at the exit of the MW-splitter cube that will be made of fused silica.

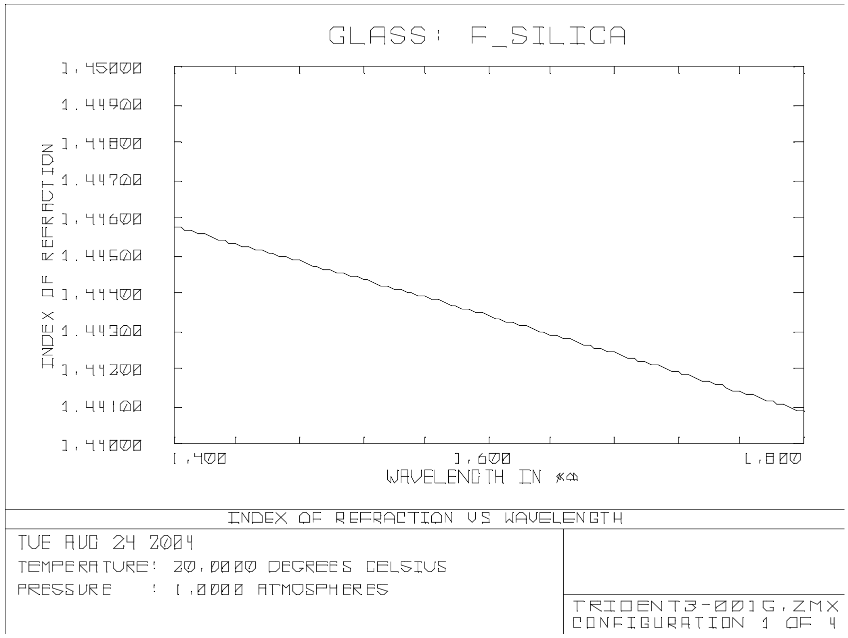

Figure 7 – Index of refraction of Fused Silica vs. Wavelength, at room temperature and pressure

6.5 MW-splitter cube

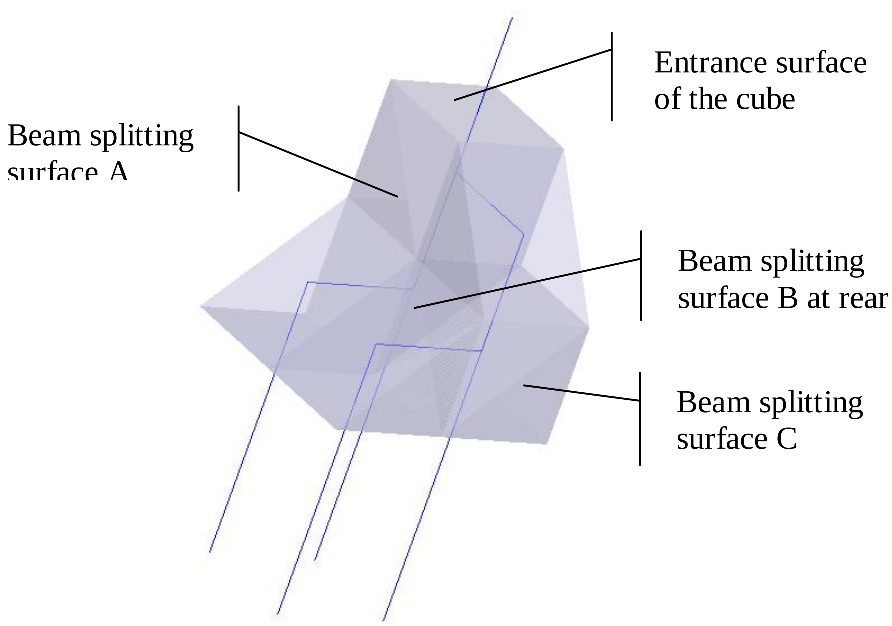

Figure 8 - 3D view of Beam Splitter Cube

* Inversed image, see Figure 9 and Figure 10 below for real orientation of surfaces.

The splitting surfaces of the MW-splitter cube are defined as:

- Beam splitting surface A: Transmitted: $1.50 < \lambda < 1.61\mu m$
  Reflected: $1.61 < \lambda < 1.72\mu m$
  the blocking of wavelengths $<1.50\mu m$ and $>1.72\mu m$ can be done on the entrance and/or exit surface or on the first beam splitting surface.
- Beam splitting surface B: Transmitted: $\lambda<1.55\mu m$
  Reflected: $\lambda>1.55\mu m$
- Beam splitting surface C: Transmitted: $\lambda<1.67\mu m$
  Reflected: $\lambda>1.67\mu m$

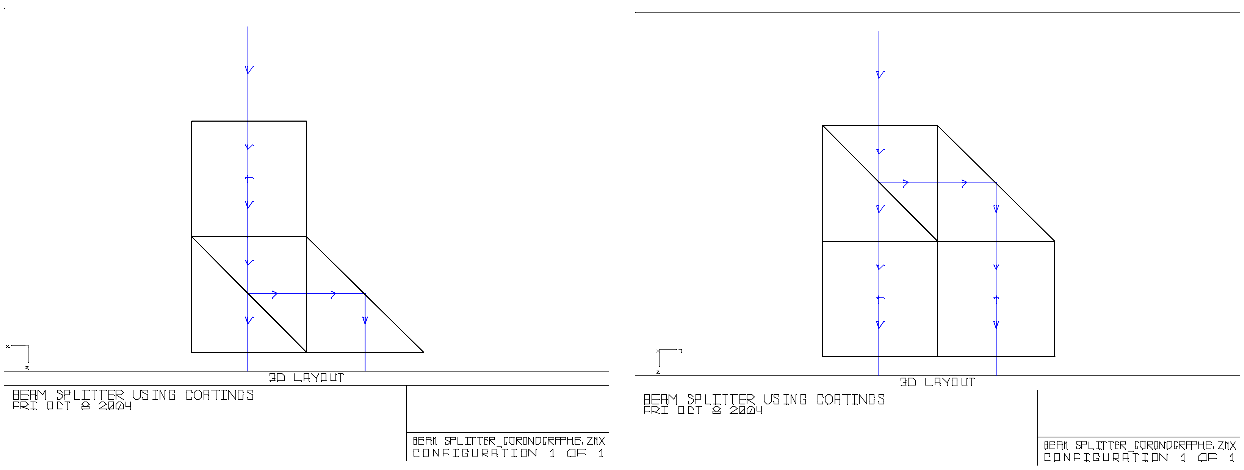

Figure 9 – Side and Front views of Beam Splitter Cube

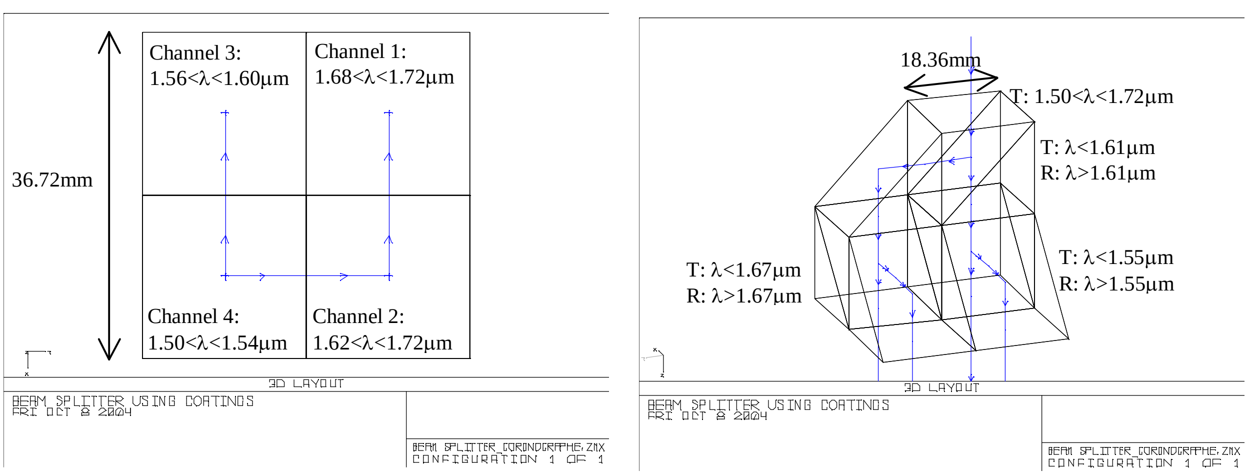

Figure 10 – Wave band for each Channel

6.6 MW-splitter coating design and considerations

The Multi-Wavelength Imager (MWI) concept relies on splitting the incoming spectral band into 4 narrower spectral bands by means of a dichroic assembly. The assembly requires edge and bandpass filter design for cryogenic temperature to cover the H-band. The following discuss the different topics about this dichroic assembly.

6.6.1 Comparison of Immersed and non-Immersed coating

	Immersed	Non-Immersed	
Damage threshold	Low	High	Presence of optical cement
Astigmatism	None	Fairly	When illuminated with convergent light
Polarisation sensitivity	High	Medium	Produce a polarisation splitting
Coating design	High	High-Medium	Caused by polarisation requirements at 45^{o} AOI
Fabrication cost	Higher	Lower	Caused by coating design

6.6.2 Definition of an Immersed coating

An immersed coating is generally obtained when the immersion constant ($L = n_o \sin(\theta_o)$) is greater that 0.95, where (θ_o) is the angle of incidence and (n_o) is the refractive index of the incidence medium upon the coating interface.

6.6.3 Specifications of edges and bandpass filters

The filter specification with the most importance is the bandwidth of the bandpass filters. Since this quantities allow more or less spectral width for the edge filters. The table below shows four calculations with different bandwidth requirement of the bandpass filter. The filter bandwidth at half maximum (BWHM) specification is illustrates in the bold bounded Yellow cells. The associated BWHM in nanometer is calculated in the Yellow cells. With these values we calculate the 50% transmittance point at the short edge (blue cells) and at the long edge (red cells) 1556.3 n bandp 1542.8 er. = 13.5 e difference between the 1520nm first bandpass filter 50% long edge transmittance point and the 1580nm second bandpass filter 50% short edge transmittance point gives us the spectral width ($\Delta\lambda$) of adjacent filter (orange cells).

This is the wavelength span allowed where the edge filters must undergo the transition between high and low transmission. It can also be used as the maximum tolerance specified on the 50% transmission point of the edge filter for the coating vendor. Another quantity of interest for the edge filter fabrication is the slope that is inversely proportional to the steepness of the edge transition between high and low transmission values. A short wave pass edge filter slope is defined by the following: $S = 100 * (\lambda_{T5} - \lambda_{T80})/\lambda_{T5}$ and a long wave pass edge filter slope is $S = 100 * (\lambda_{T80} - \lambda_{T5})/\lambda_{T5}$ with λ_{T5}

being the cut-on wavelength at the absolute 5% transmittance value and λ_{T80} being the wavelength at 80% of the mean pass band transmittance. For the purpose of the actual evaluation we took the 50% transmittance wavelength point (λ_{T50}) of 2 adjacent bandpass filters as being the λ_{T80} and λ_{T5} for the edge filter slope calculation as shown at figure 1.

$$100 * \frac{(1556.3 - 1542.8)}{1556.3} = 0.86744201$$

We can clearly see that the edge filter slope is larger than 1% for bandpass filter with less that 2% BWHM. According to Phillip W. Beaumeister, "Optical coating technology" reference book, edge filter with slope larger than 5% are easy to fabricate and slope less than 2% require "*exceedingly precise control of the process*".

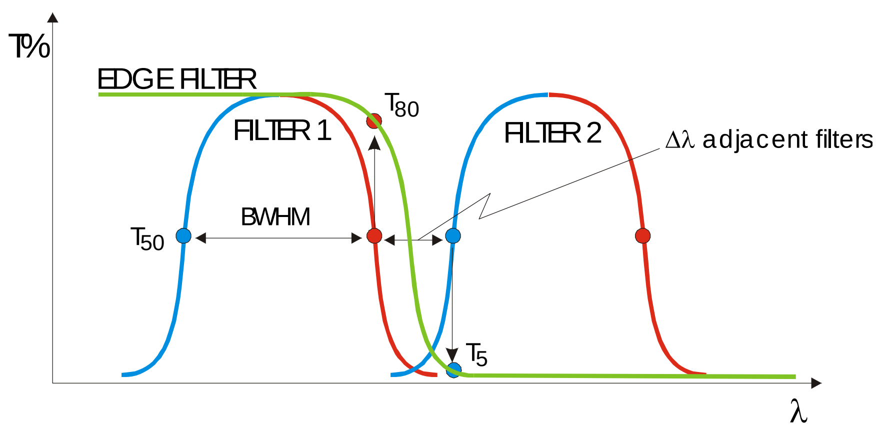

Figure 11 – illustration of edge and bandpass filter terminology for the MWI.

λ central filter (nm)			1520		1580		1640		1700	
Δλ central (nm)				60		60		60		
BWHM	3%		45.6		47.4		49.2		51	
50% short edge (nm)		1497.2		1556.3		1615.4		1674.5		
50% long edge (nm)				1542.8		1603.7		1664.6		1725.5
Δλ of adjacent filter at 50% (nm)				13.5		11.7		9.9		
Slope of edge filter (%)				0.8674		0.7243		0.5912		

λ central filter (nm)			1520		1580		1640		1700	
Δλ central (nm)				60		60		60		
BWHM	2%		30.4		31.6		32.8		34	
50% short edge (nm)		1504.8		1564.2		1623.6		1683		
50% long edge (nm)				1535.2		1595.8		1656.4		1717
Δλ of adjacent filter at 50% (nm)				29		27.8		26.6		
Slope of edge filter (%)				1.854		1.7122		1.5805		

λ central filter (nm)			1520		1580		1640		1700	
Δλ central (nm)				60		60		60		
BWHM	1.5%		22.8		23.7		24.6		25.5	
50% short edge (nm)		1508.6		1568.2		1627.7		1687.3		
50% long edge (nm)				1531.4		1591.9		1652.3		1712.8
Δλ of adjacent filter at 50% (nm)				36.75		35.85		34.95		
Slope of edge filter (%)				2.3435		2.2025		2.0714		

λ central filter (nm)			1520		1580		1640		1700	
Δλ central (nm)				60		60		60		
BWHM	1%		15.2		15.8		16.4		17	
50% short edge (nm)		1512.4		1572.1		1631.8		1691.5		
50% long edge (nm)				1527.6		1587.9		1648.2		1708.5
Δλ of adjacent filter at 50% (nm)				44.5		43.9		43.3		
Slope of edge filter (%)				2.8306		2.6903		2.5599		

Table 1 Calculation for edge and bandpass filter specifications

6.6.4 Edge filter specifications of commercial vendor

We consulted three thin film vendors specialized in filter fabrication for their standard specification available from WEB advertising.
The first company, Spectrogon, has the following specification for long wave pass filter between 1.4 to 1.7 µm.

accuracy on cut-on wavelength (λ_{T5})	+/- 30 nm to +/- 50 nm
Slope	≈ 5 %
Average transmittance	≥ 75 %
Average reflectance	≥ 99 %

The second company, Andover Corp., has the following specification for long wave pass filter below 1.0 μm.

accuracy on cut-on wavelength (λ_{T5})	+/- 10 nm
Slope	≈ 6 %
Average transmittance	≥ 80 %
Average reflectance	> 99 %

The last one, OCLI, has the following specification for their long wave pass filter between 1 to 3 μm.

accuracy on cut-on wavelength (λ_{T5})	Not found
Slope	3% to 6 %
Average transmittance	≥ 85 %
Average reflectance	Not found, but T ≤ 0.1%

At Barr associate, there is no commercial specifications available but they indicate that "*Typical slope for an edge filter with steep slope would be 1%* ", which shows their capabilities to achieve such specification.

6.6.5 Example of non-polarized Edge filter

Here below an example of a non-polarized edge filter at 20 degrees angle of incidence. It is a modified version of Thelen 's edge filter at non-normal incidence in "Design of Optical interference coating, Chap 9, p. 194" .

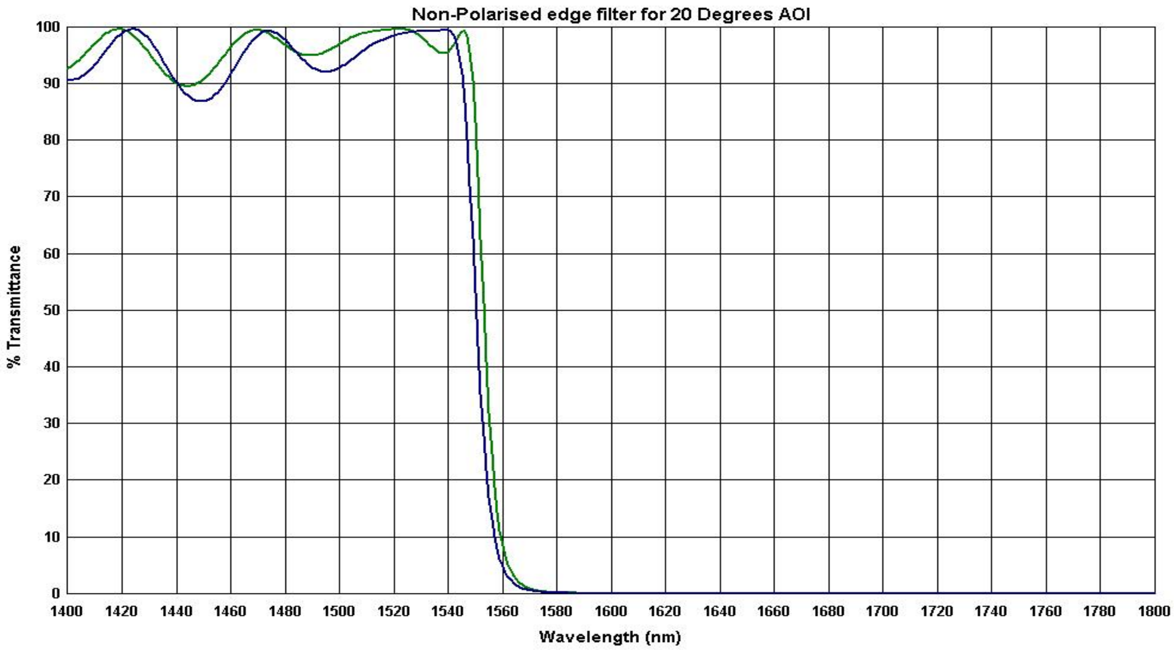

Figure 12 – Non-polarized edge filter at 20 degrees angle of incidence (green curve: P-pol., Blue curve: S-pol.)

The thin film design at figure 2 in is a non-immersed design, not yet suitable for MWI dichroic assembly. However with it 96 layers count and slope of 0.72% for p-polarization, it illustrates difficulties that thin film designer would have to overcome to increase the angle of incidence to 45^{o} in an immersed design.

Thin film design of figure 2: glass/.2752H .3467L .2752H .9143H .1867L .788H .1867L .9143H (.732H .4648L .468H .4648L .732H)2 (.6153H .7847L .19H .7847L .6153H)12 (.732H .4648L .468H .4648L .732H)2 .9143H .1867L .788H .1867L .9143H .1678H .5613L .1678H/air
(Glass :1.52, n_H = 3.5, n_L = 1.45, λ_{design} = 1210 nm, QWOT =1)

6.6.6 Phase variation across edge filter

The phase variation across such edge filter design must be carefully considered since large phase shift either in transmission or reflection occurs as shown below for the thin film design of figure 2.

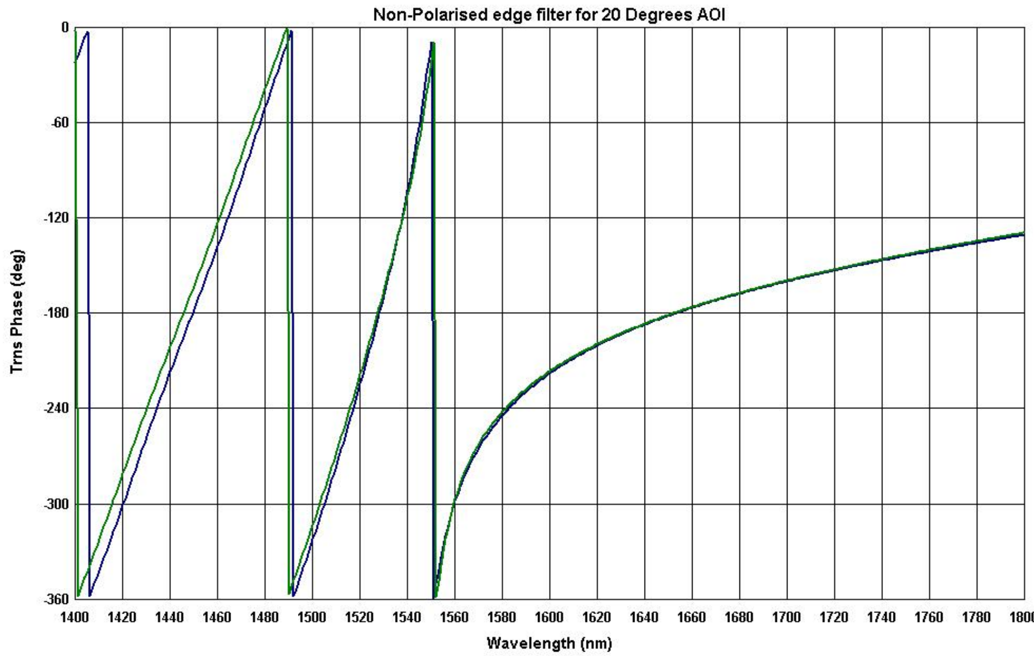

Figure 13 – Transmitted phase for thin film design of figure 2. (green curve: P-pol., Blue curve: S-pol.)

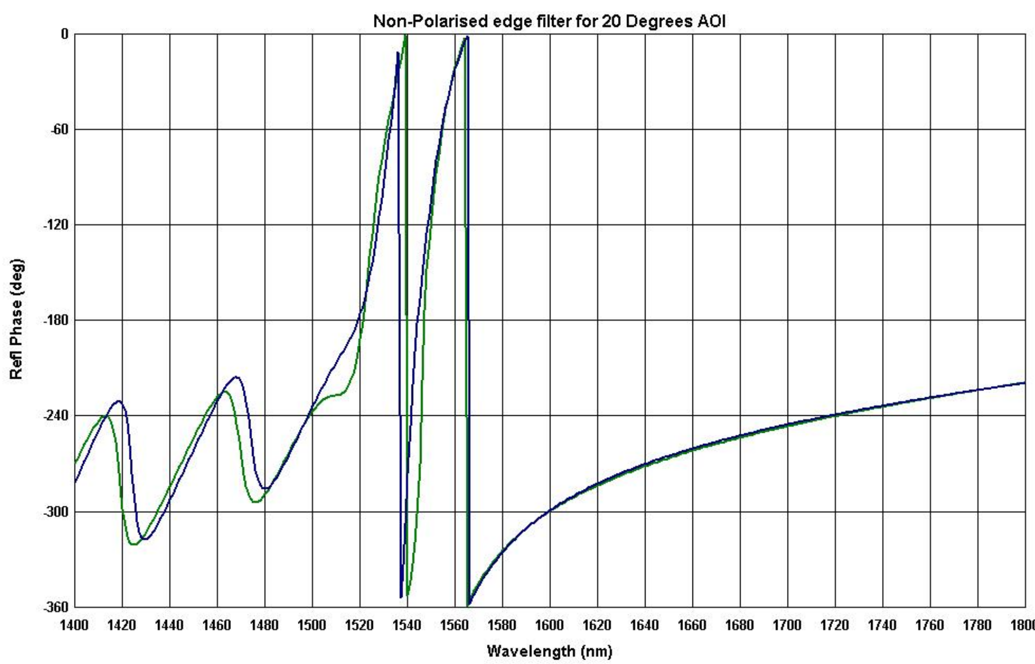

Figure 14 – Reflected phase for thin film design of figure 2. (green curve: P-pol., Blue curve: S-pol.)

6.7 Fore Optic Converter Design

The output of the coronagraph will be a 15 mm collimated beam (from an F/64 off axis parabola). The fore optic converter (FOC) includes the cryostat window, the cold pupil (15 mm) and an off axis parabola (OAP) focusing element that produce an F/90 image plane.

The FOC design is not shown due to its simplicity. We have also to consider mechanical constraint about the size of the instrument that led the design by introducing appropriates folding mirrors. The base line is shown in the following figure.

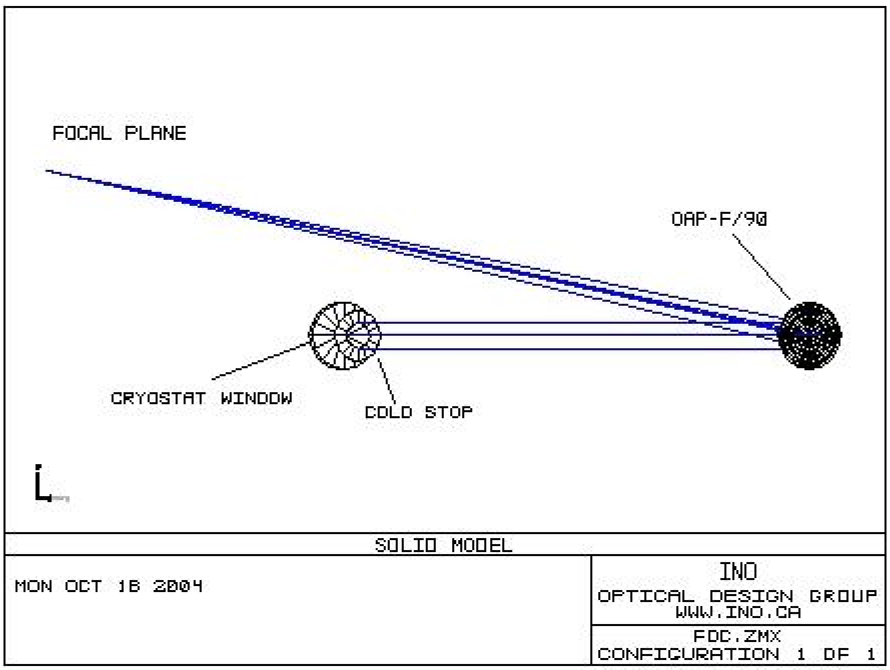

Figure 15 – FOC optical layout (unfolded)

6.8 Input Image Condition

The input image is the lenslet array. We assume a unit magnification, so the lenslet array is a square of 18mm width. The input beam F/# is 5.6 (NA=0.0889) and the object space is telecentric.

6.9 Lenslet array

The lenslet array is a square shape, 54 µm pitch (= 3 detector pixels assuming unit magnification), f/5.6 output corresponding to λf/D~9 µm or half a detector pixel. The sag is shown in the following figure.

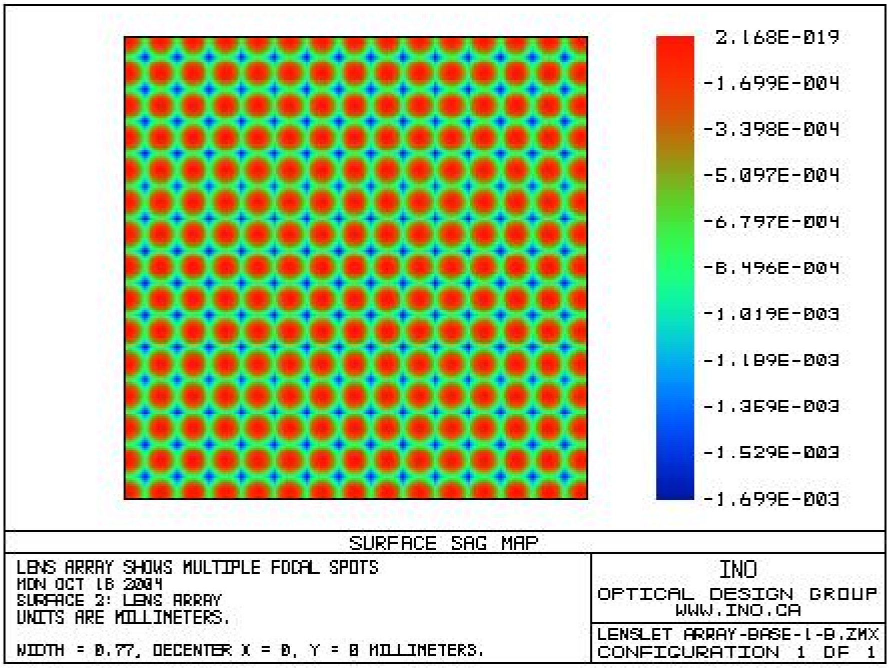

Figure 16 – Lenslet array sag (part of the aperture)

The sag of the lenslet is quite small which allows us to use many suppliers to build such lenses. One potential supplier is INO micro-optics group. They use a laser writer system to write a master of the lenslet array. After this step, a solgel replicated element can be built (or many for a fraction of the cost).

6.9.1 Fabrication Process with Sol-Gel Microlens

- Bonded Process for Sol-Gel Microlens

(Here, the photopolymer material will be our Sol-Gel Glass)

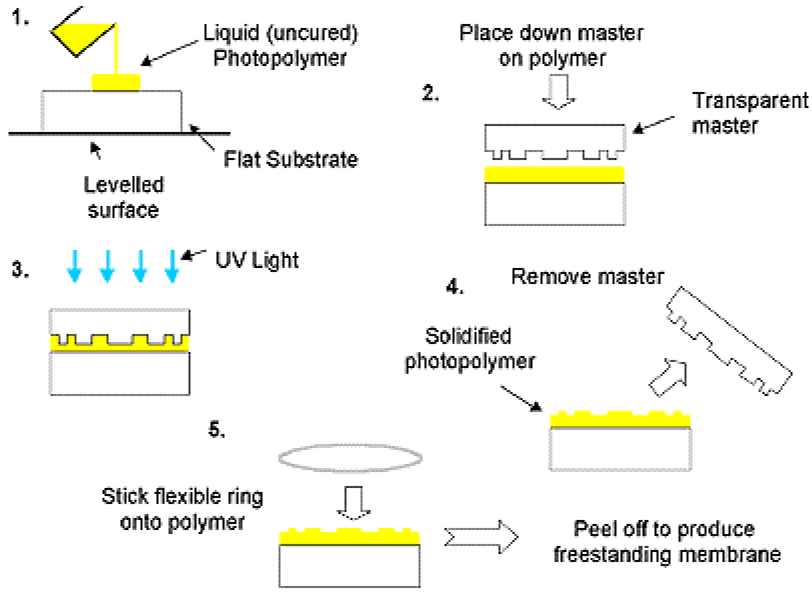

The replication process reproduces the contacted surfaces very well, with a uniform ~1% shrinkage over the part. Over smaller sizes, microlens, micron-scale gratings and smooth, refractive surfaces etc have also been replicated successfully.

- Sol-gel glass is hybrid organic-inorganic material or hybrid glass material. It contains a polymeric part for UV photopolymerization and high thickness capability, as well as a SiO2 structure for rigidity. It's fully transparent in visible and near IR passband, and it has a good thermo-mechanical stability.
- The withstand mechanical shock/vibration as well as thermal shock from – 45 deg C to 85 deg C, the behavior of the sol-gel microlens is very similar to the conventional SiO2 lens (silica lens). We have run the required environment and thermal tests for these lenses in order for some projects and customers before. It's great.
- Laser power handling issue: We have run some tests for our clients as they requested in their applications before. The obtained data of the Laser Power Damage Threshold for our sol-gel glass is given below as your reference:
  1) Test wavelength = **1064 nm, 14 ns, 1Hz, applied 30sec**.:
  Sol-gel glass + AR coating: damage threshold = 2 to 4 Joule /cm^2
  (≥143 MW/cm^2)
  2) Test wavelength **= 808 nm, 40 ms, 4Hz, tested for 2500 hrs.**
  with 110J/cm^2, => 2.75 MW/ cm^2
  Sol-gel glass + AR coating: no damage recorded

6.10 Imager Optical Design

6.10.1 General Layout FFOV Optical Design

FFOV, 18mmX18mm relay design using 11 custom lenses (the bandpass filter is not shown).

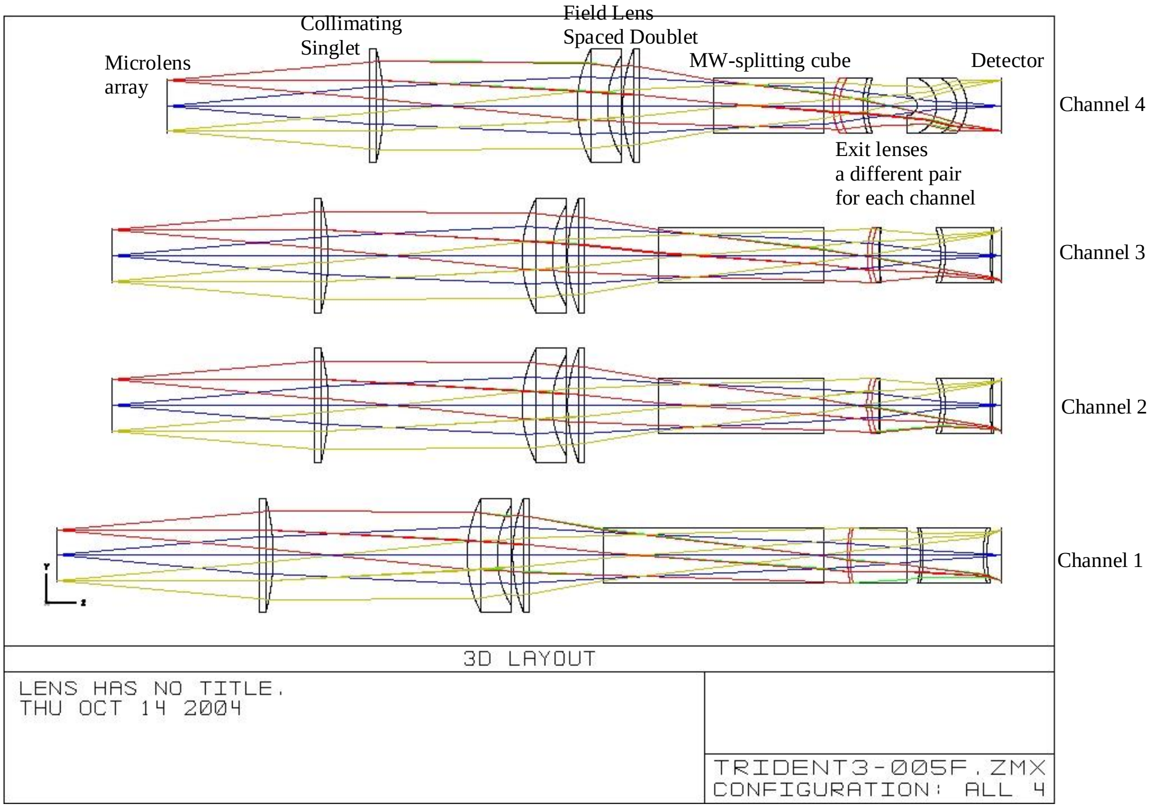

Figure 17 – Side view of design with optical path into each channel of the MW-splitting cube

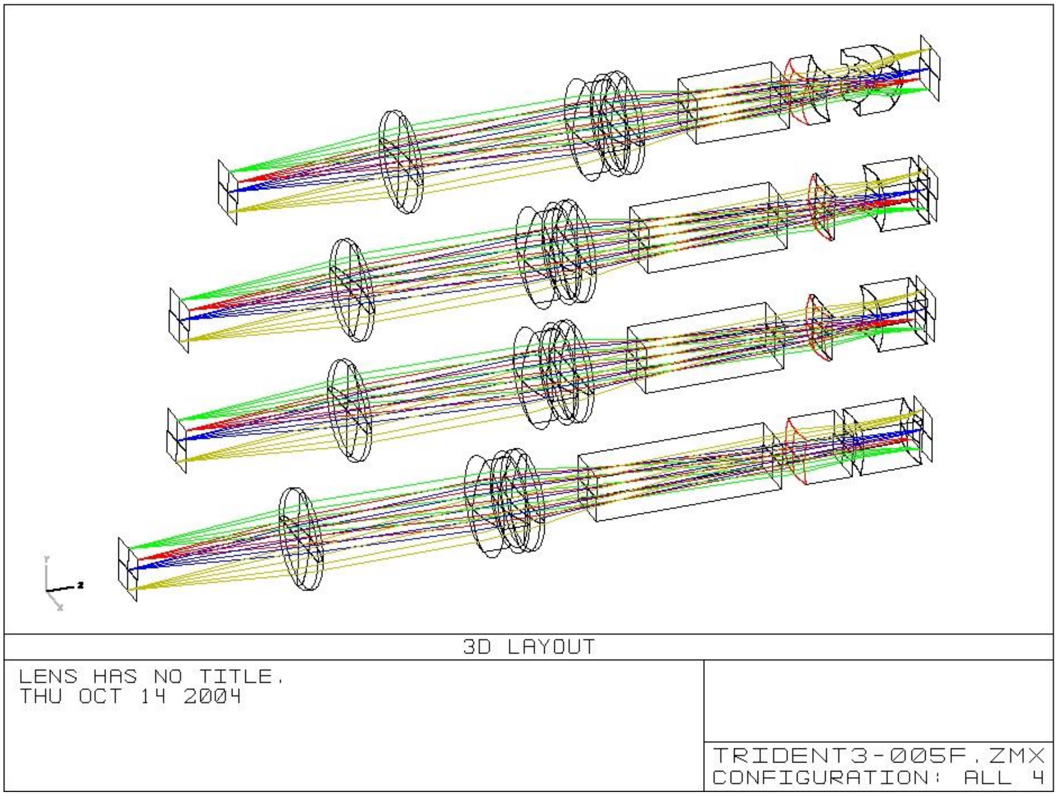

Figure 18 – 3D view of design with optical path into each channel of the MW-splitting cube

6.10.2 General Layout MFOV Optical Design

It is possible to simplify the design by replacing similar exit lenses by identical ones. Instead of using 11 custom lenses, we can just use 8 different lenses. The image quality degrades slightly; the RMS spot size gets slightly larger on the outside of the field for each channel.

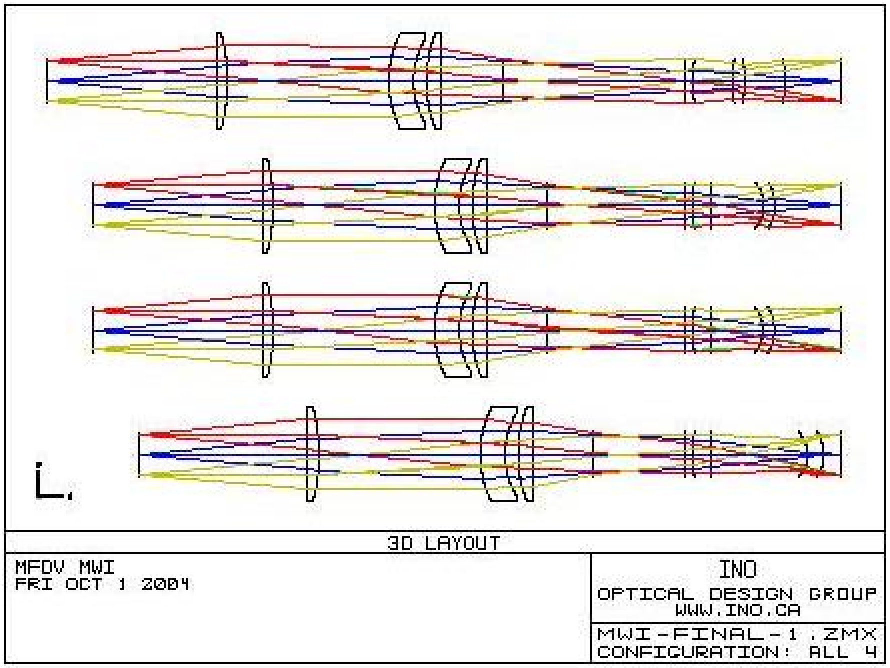

Figure 19 - MFOV, 16mmX16mm relay design using 8 custom lenses.

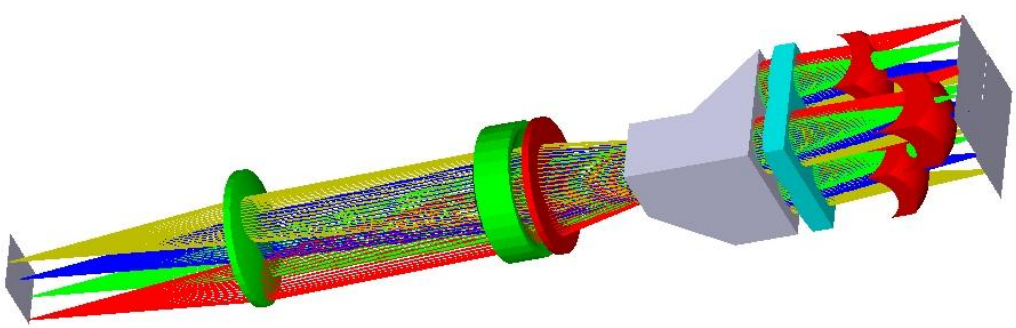

Figure 20 - 3D layout of the MWI (MFOV)

6.10.3 FFOV Optical prescription

Lens	Channel	Material	Spacing / Center thickness (mm)	R1 (mm)	R2 (mm)
Lenslet Array					
Spacing	All		64.57		
Singlet	All	BaF2	4.50	∞	-74.14
Spacing	All		64.70		
Doublet A	All	BaF2	10.00	41.80	32.60
Spacing	All		5.17		
Doublet B	All	SF6	5.60	5.02	∞
Spacing	All		24.70		
Cube	1	Fused Silica	73.44	∞	∞
	2		55.08		
	3		55.08		
	4		36.72		
Spacing	1		7.81		
	2		14.33		
	3		14.45		
	4		3.00		
Exit lens 1	1	SF6	20.00	45.87	∞
	2	BaF2	4.00	28.63	165.54
	3		4.00	28.37	154.42
	4		10.00	20.61	28.10
Spacing	1		5.30		
	2		22.10		
	3		22.00		
	4		24.60		
Exit lens 2	1	SF6	20.00	-46.29	36.37
	2		15.00	-28.51	71.76
	3		15.00	-28.49	74.90
	4	BaF2	10.00	-9.72	-14.14
Spacing	1		6.28		
	2		3.96		
	3		3.93		
	4		11.79		
Detector					

6.11 Image Quality

If we consider a square lenslet array, of 18 mm width:

Channel No.	Wavelength (μm)	Airy diameter (μm)	*Spot size RMS radius, referenced to centroid (μm) / Coordinates(X,Y) on the image plane (mm)*		
			Field 1 /Coord. (0,0)	*Field 2 /Coord. (0,9)*	*Field 3 /Coord. (9,9)*
1	1.70	23.27	6.869 / (0,0)	10.038 / (0,-8.996)	13.214 / (-9.000,-9.000)
2	1.64	22.44	6.514 / (0,0)	6.793 / (0,-8.999)	9.624 / (-8.998,-8.998)
3	1.58	21.62	6.459 / (0,0)	6.885 / (0,-8.999)	9.700 / (-8.999, -8.999)
4	1.52	20.79	5.443 / (0,0)	13.017 / (0,-9.011)	20.999 / (-8.996,-8.996)

If we reduce the lenslet array and the input field to a circle of 16mm diameter instead of a square of 18mm width, we obtain, for the same design, the following RMS spot radius:

Channel No.	Wavelength (μm)	Airy diameter (μm)	*Spot size RMS radius, referenced to centroid (μm) / Coordinates(X,Y) on the image plane (mm)*		
			Field 1 /Coord. (0,0)	*Field 2 /Coord. (0,8)*	*Field 3 /Coord. (5.657,5.657)*
1	1.70	23.27	6.869 / (0,0)	9.165 / (0,-7.998)	9.165 / (-5.654,-5.654)
2	1.64	22.44	6.514 / (0,0)	6.773 / (0,-7.998)	6.773 / (-5.655,-5.655)
3	1.58	21.62	6.459 / (0,0)	6.860 / (0,-7.998)	6.860 / (-5.655,-5.655)
4	1.52	20.79	5.443 / (0,0)	11.179 / (0,-8.005)	11.179 / (-5.660,-5.660)

The magnification is 1 at the center of the field, between 0.999556 and 1.001222 at the edge of the field on the x and y axis and 0.999556 and 1 at the edge of the field on the diagonals. The distortion of the image at the edge of the field shifts a spot of +3/-4 μm from its nominal position. That is inside the half pixel width of 9μm.

For the simplified design, the same analysis can be done. If we consider a square lenslet array, of 18 mm width:

Channel No.	Wavelength (μm)	Airy diameter (μm)	*Spot size RMS radius, referenced to centroid (μm) / Coordinates(X,Y) on the image plane (mm)*		
			Field 1 /Coord. (0,0)	*Field 2 /Coord. (0,9)*	*Field 3 /Coord. (9,9)*
1	1.70	23.27	5.009 / (0,0)	8.158 / (0,-8.965)	17.443 / (-8.908,-8.908)
2	1.64	22.44	9.200 / (0,0)	11.209 / (0,-9.037)	19.631 / (-9.029,-9.029)
3	1.58	21.62	8.791 / (0,0)	11.302 / (0,-9.039)	19.408 / (-9.031, -9.031)
4	1.52	20.79	10.586 / (0,0)	13.349 / (0,-9.050)	20.673 / (-9.050,-9.050)

The magnification is 1 at the center of the field, between 0.996111 and 1.005556 at the edge of the field on the x and y axis and 0.989778 and 1.005556 at the edge of the field on the diagonals. The distortion at the edge of the field shifts a spot of +50/-92 μm from its nominal position. That is about five pixels width.

If we reduce the lenslet array and the input field to a circle of 16mm diameter instead of a square of 18mm width, we obtain, for the same design, the following RMS spot radius:

Channel No.	Wavelength (μm)	Airy diameter	*Spot size RMS radius, referenced to centroid (μm) / Coordinates(X,Y) on the image plane (mm)*

		(μm)	*Field 1 /Coord. (0,0)*	*Field 2 /Coord. (0,8)*	*Field 3 /Coord. (5.657,5.657)*
1	1.70	23.27	5.009 / (0,0)	7.792 / (0,-7.974)	7.792 / (-5.639,-5.639)
2	1.64	22.44	9.200 / (0,0)	10.931 / (0,-8.034)	10.931 / (-5.681,-5.681)
3	1.58	21.62	8.791 / (0,0)	10.934 / (0,-8.036)	10.934 / (-5.682,-5.682)
4	1.52	20.79	10.586 / (0,0)	12.193 / (0,-8.045)	12.193 / (-5.688,-5.688)

The magnification is 1 at the center of the field, between 0.956750 and 1.005625 at the edge of the field on the x and y axis and 0.996816 and 1.005476 at the edge of the field on the diagonals. The distortion at the edge of the field shifts a spot of +45/-26 μm from its nominal position. That is two to three pixels width.

6.11.1 RMS spot size

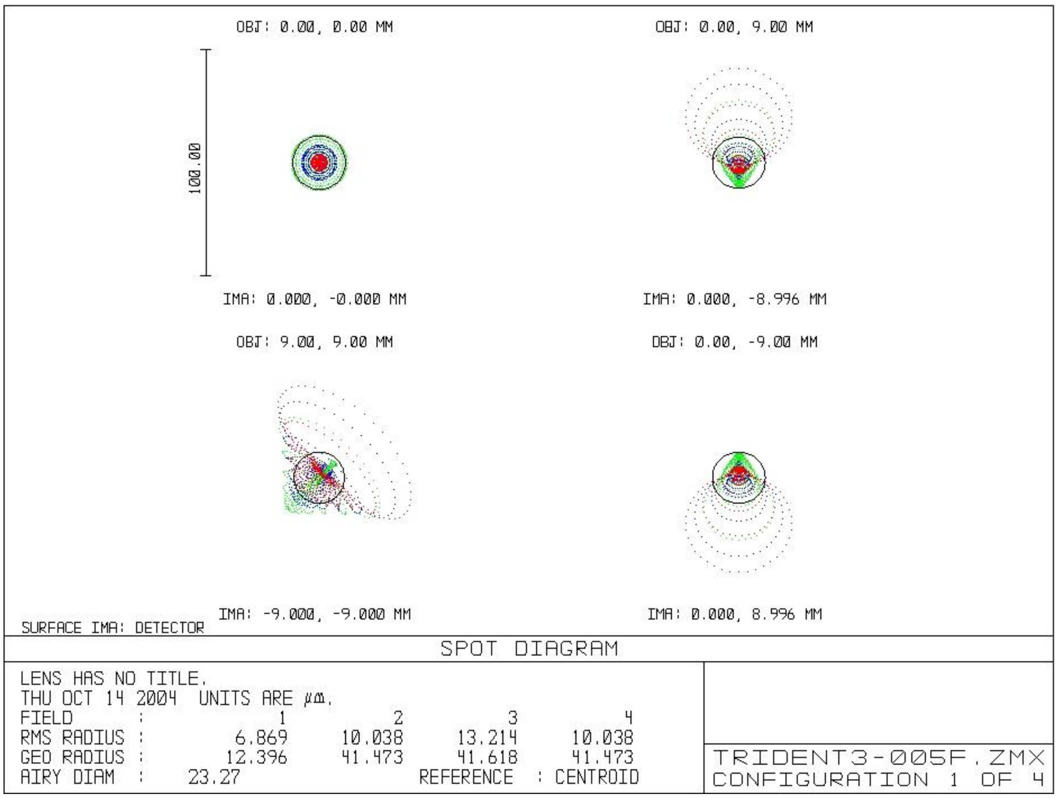

Figure 21 - RMS Spot size Channel 1

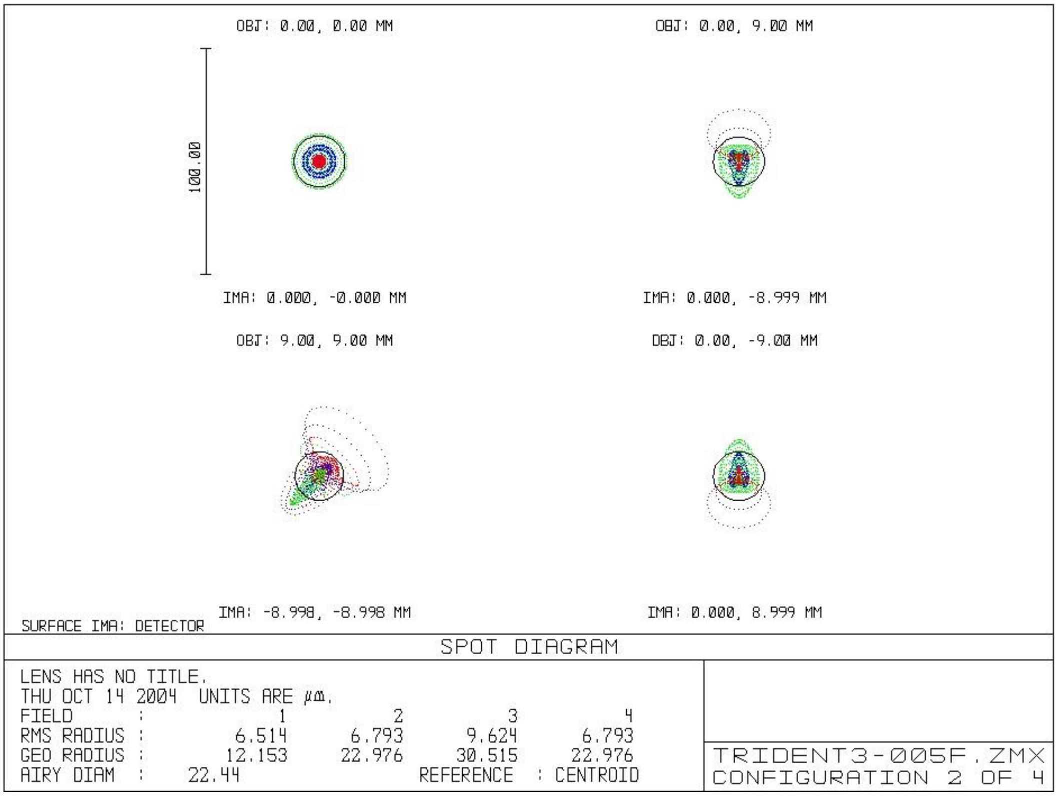

Figure 22 - RMS Spot size Channel 2

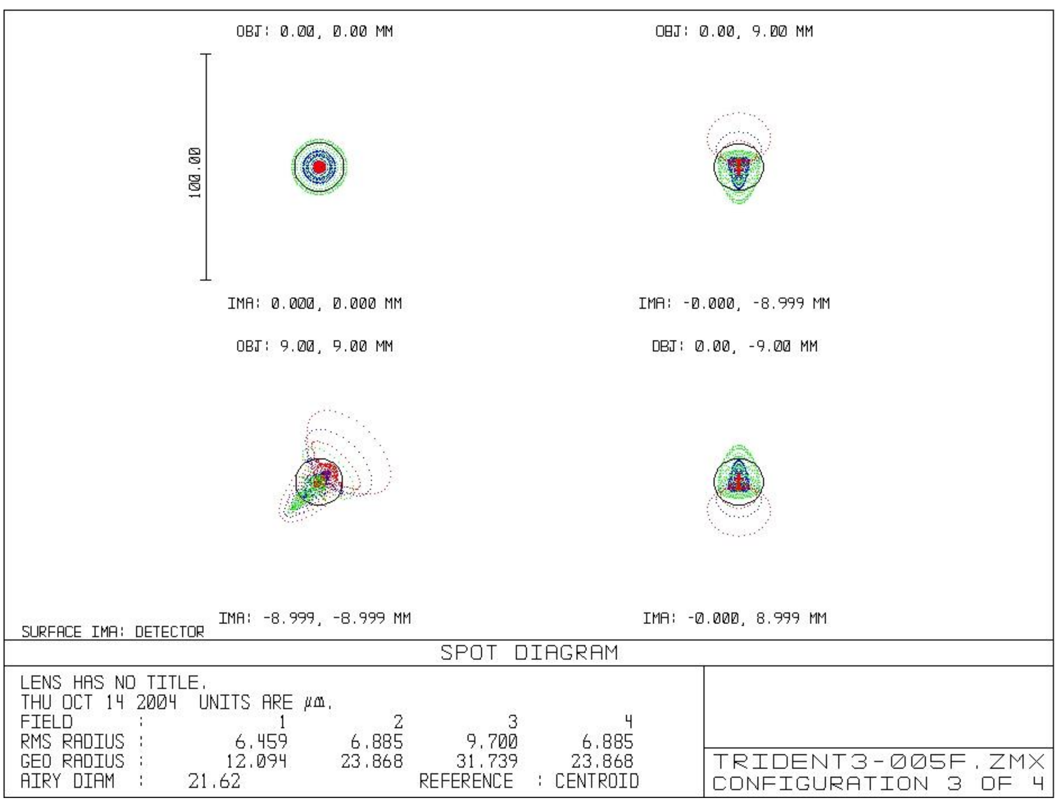

Figure 23 - RMS Spot size Channel 3

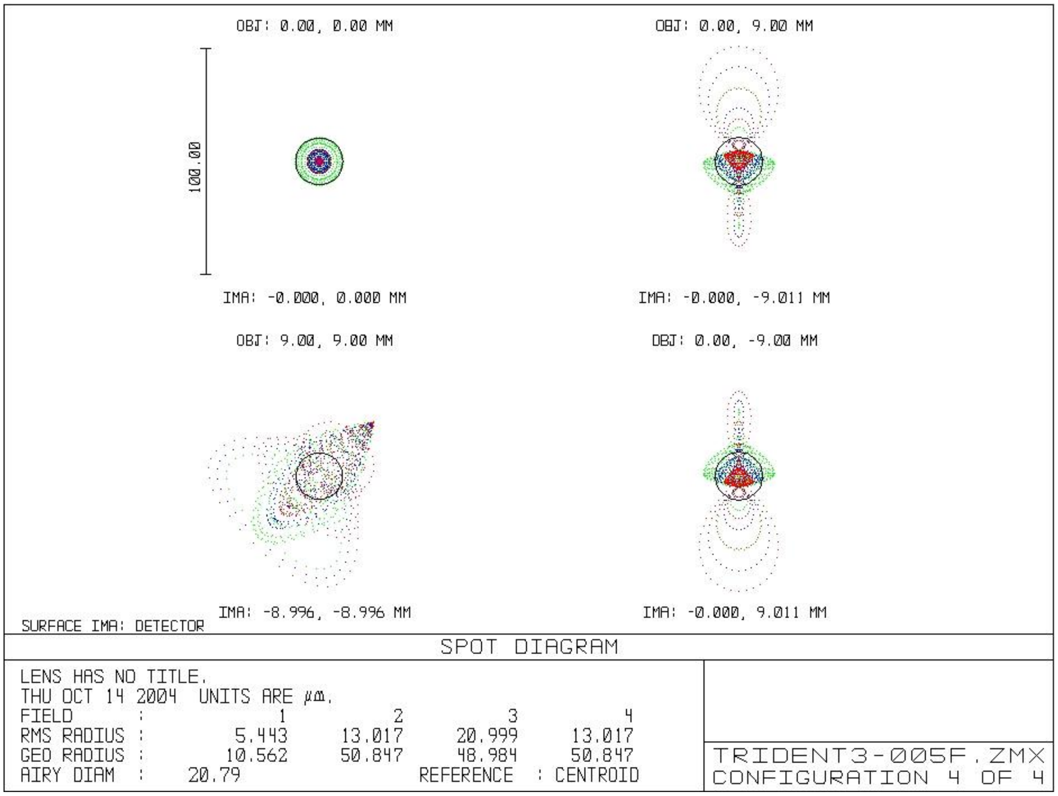

Figure 24 - RMS Spot size Channel 4

6.11.2 Wavefront

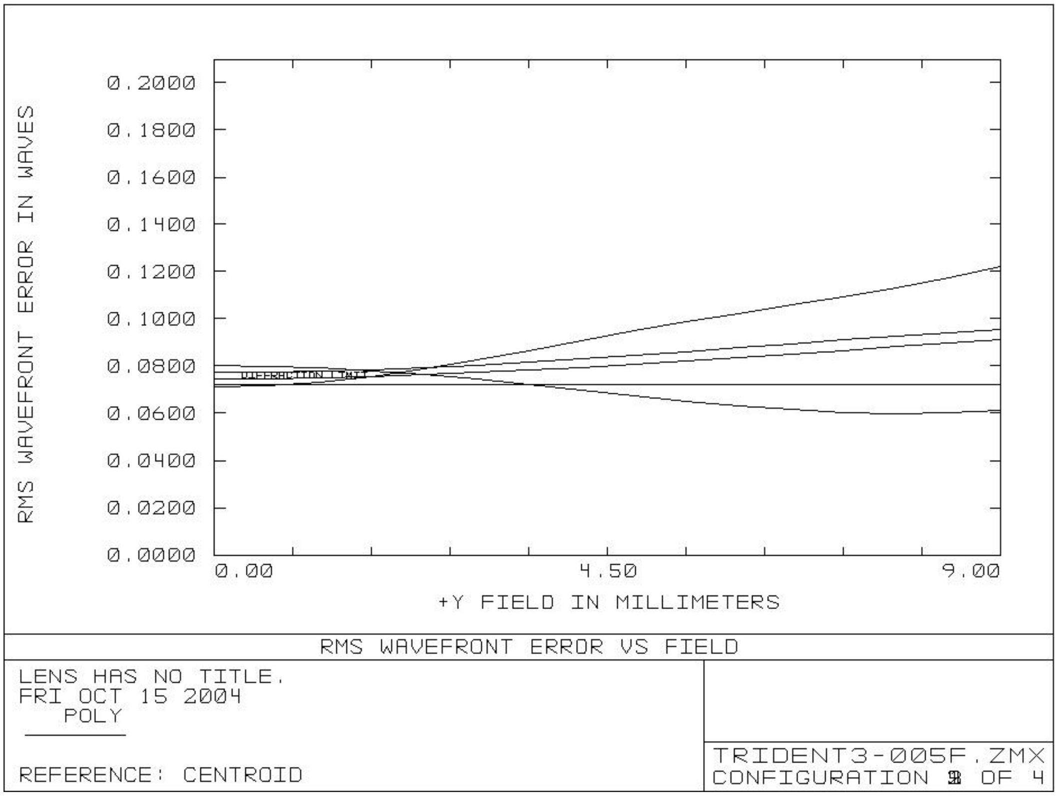

6.11.3 Strehl Ratio

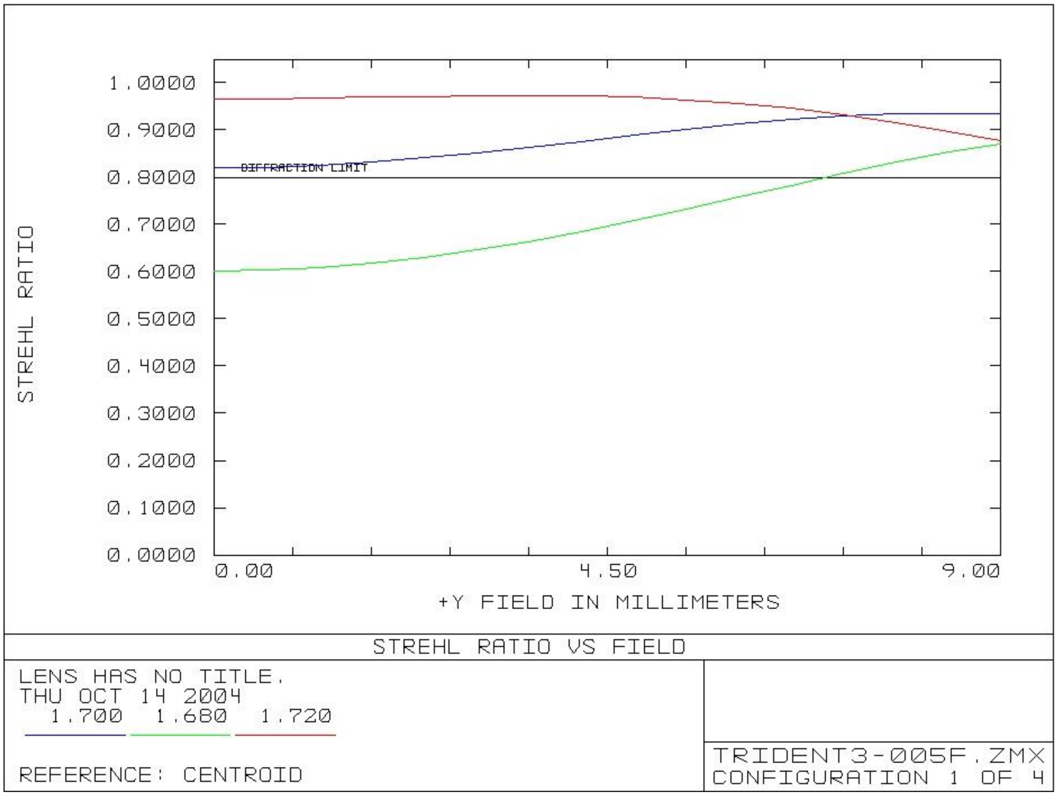
1.0000
0.9000
0.8000
0.7000
0.6000
0.5000
0.4000
0.3000
0.2000
0.1000
0.0000
STREHL RATIO
DIFFRACTION LIMIT
0.00
4.50
9.00
+Y FIELD IN MILLIMETERS
STREHL RATIO VS FIELD
LENS HAS NO TITLE.
THU OCT 14 2004
1.700 1.680 1.720
REFERENCE: CENTROID
TRIDENT3-005F.ZMX
CONFIGURATION 1 OF 4

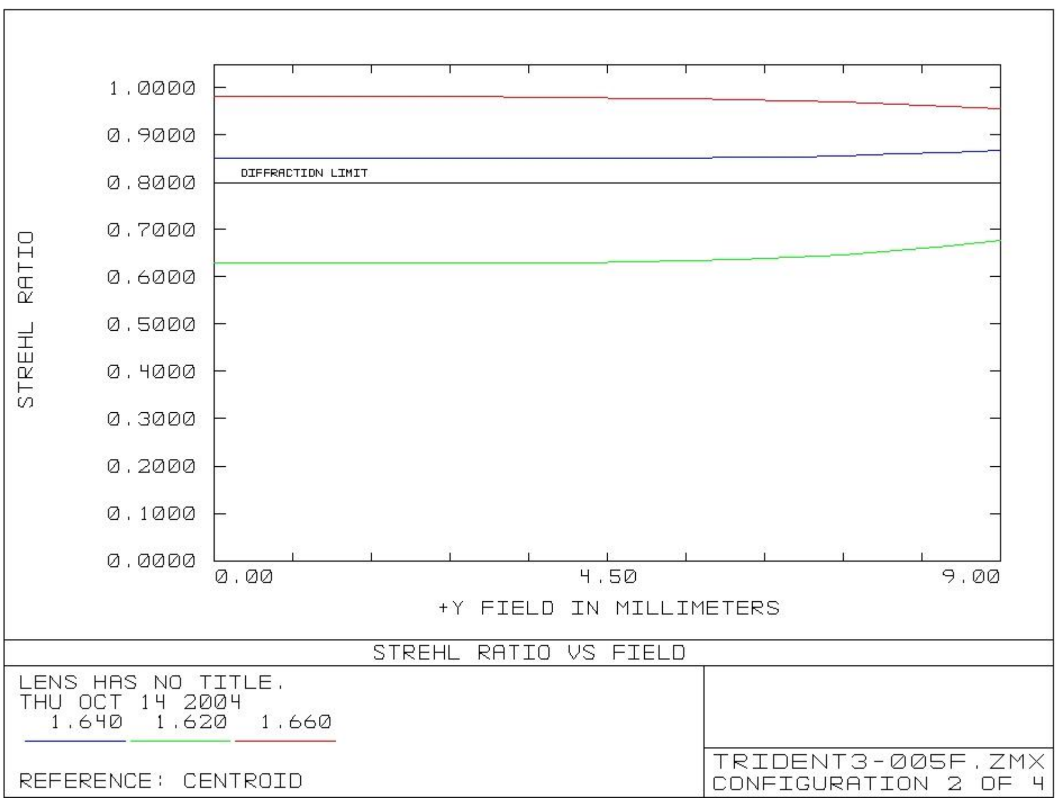
1.0000
0.9000
0.8000
0.7000
0.6000
0.5000
0.4000
0.3000
0.2000
0.1000
0.0000
STREHL RATIO
DIFFRACTION LIMIT
0.00
4.50
9.00
+Y FIELD IN MILLIMETERS
STREHL RATIO VS FIELD
LENS HAS NO TITLE.
THU OCT 14 2004
1.640 1.620 1.660
REFERENCE: CENTROID
TRIDENT3-005F.ZMX
CONFIGURATION 2 OF 4

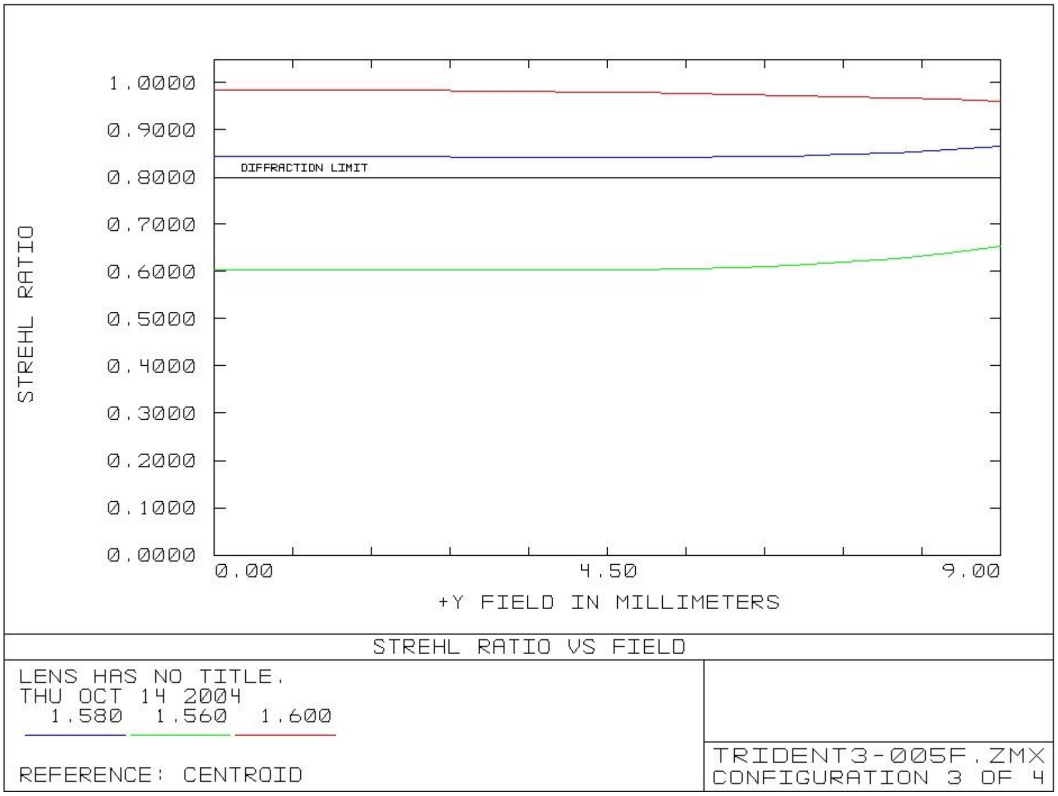
1.0000
0.9000
0.8000
0.7000
0.6000
0.5000
0.4000
0.3000
0.2000
0.1000
0.0000
STREHL RATIO
DIFFRACTION LIMIT
0.00
4.50
9.00
+Y FIELD IN MILLIMETERS
STREHL RATIO VS FIELD
LENS HAS NO TITLE.
THU OCT 14 2004
1.580 1.560 1.600
REFERENCE: CENTROID
TRIDENT3-005F.ZMX
CONFIGURATION 3 OF 4

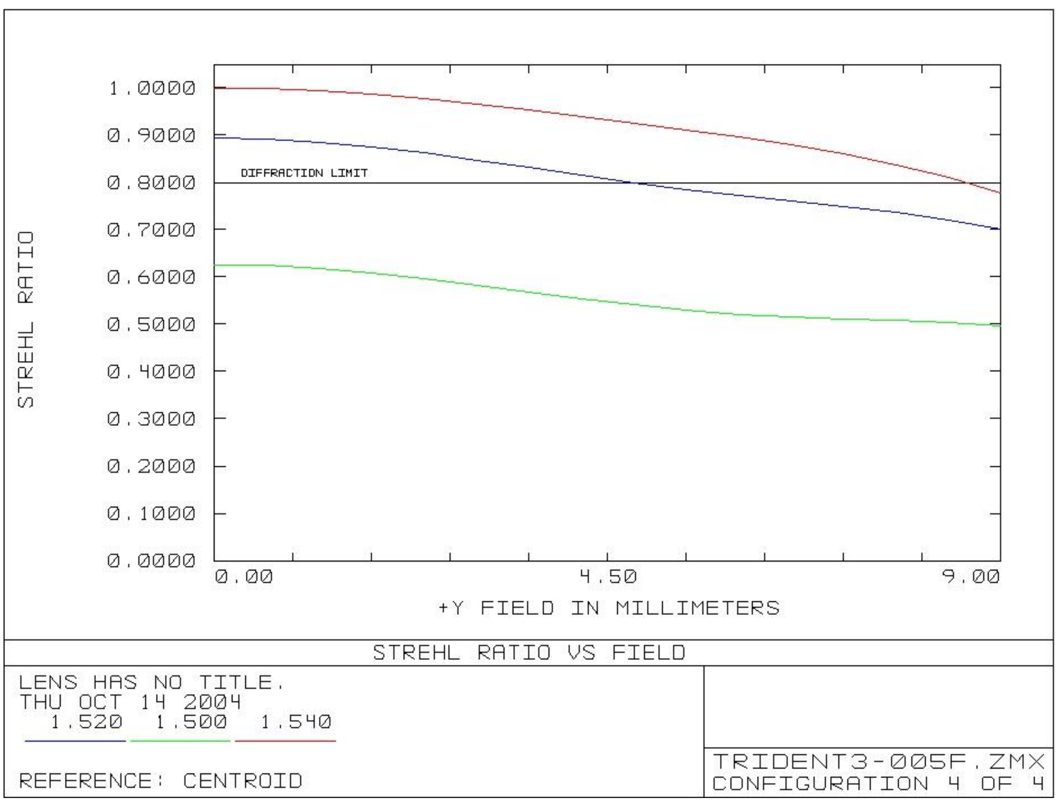
1.0000
0.9000
0.8000
0.7000
0.6000
0.5000
0.4000
0.3000
0.2000
0.1000
0.0000
STREHL RATIO
DIFFRACTION LIMIT
0.00
4.50
9.00
+Y FIELD IN MILLIMETERS
STREHL RATIO VS FIELD
LENS HAS NO TITLE.
THU OCT 14 2004
1.520 1.500 1.540
REFERENCE: CENTROID
TRIDENT3-005F.ZMX
CONFIGURATION 4 OF 4

6.11.4 Magnification and Distortion

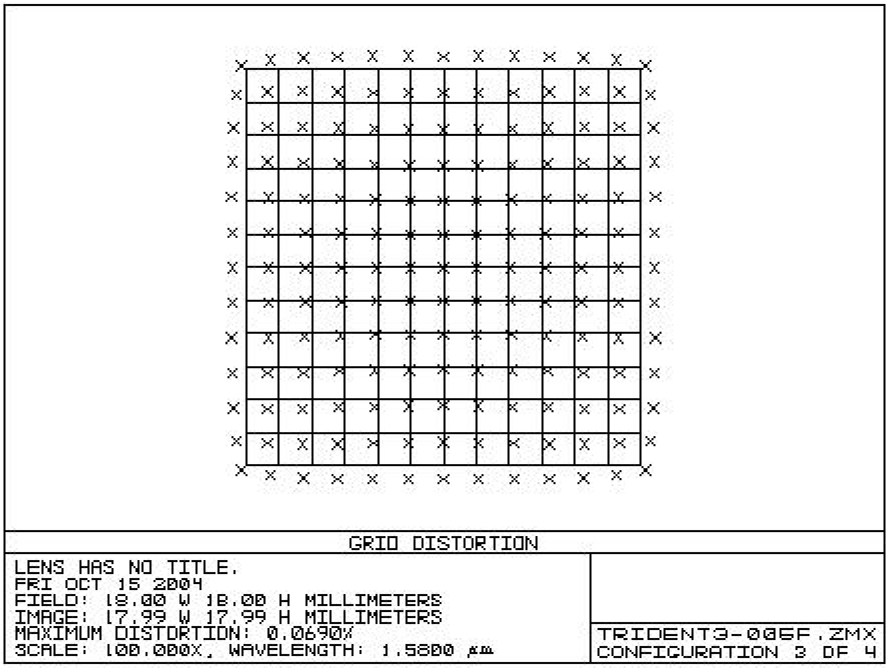

Figure 25 - Grid distortion for channel 3 at a wavelength of 1.58 μm with deviations amplified by 100. Maximum distortion is 0.06 pixel.

The distortion for channel 3 is 1µm or 0.06 pixel, and in the worst case (channel 4), 4 µm or 0.22 pixel.

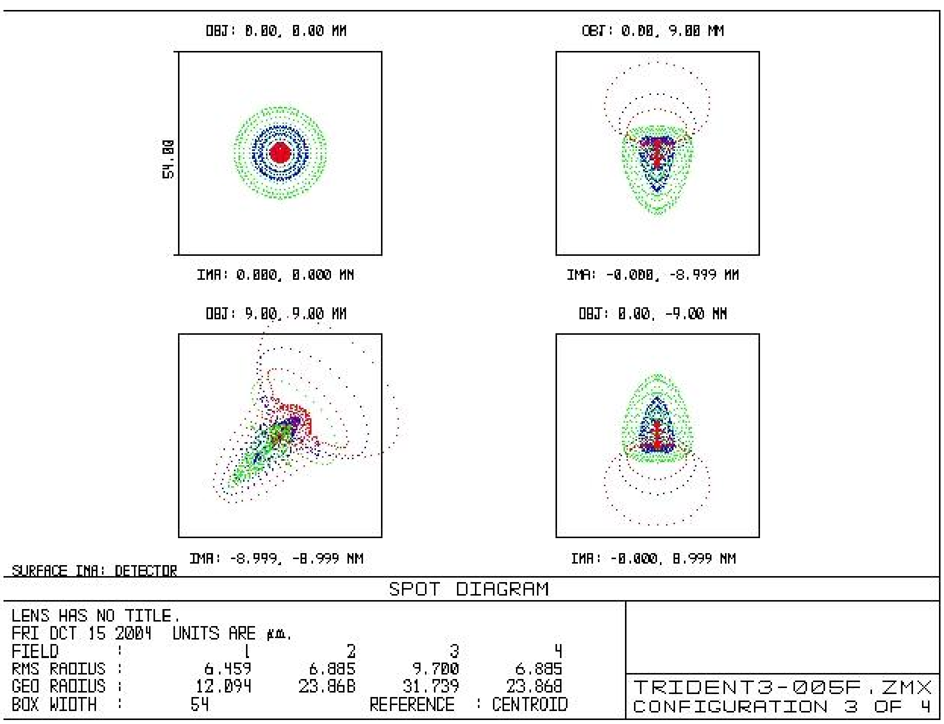

Figure 26 - Spot diagrams for channel 3 (wavelength = 1.58µm). Boxes are 3 pixels wide.

The maximum distortion over the whole field stays under 0.1% for the Channels 1 to 3, and under 0.4% for channel 4.

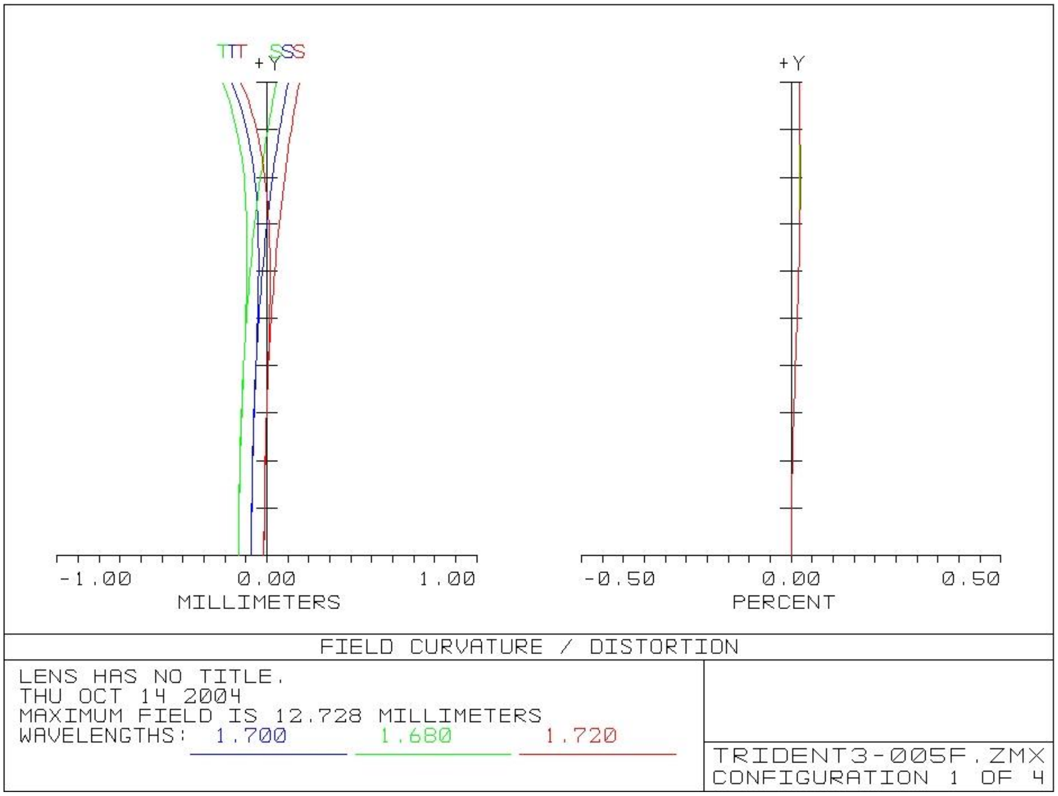

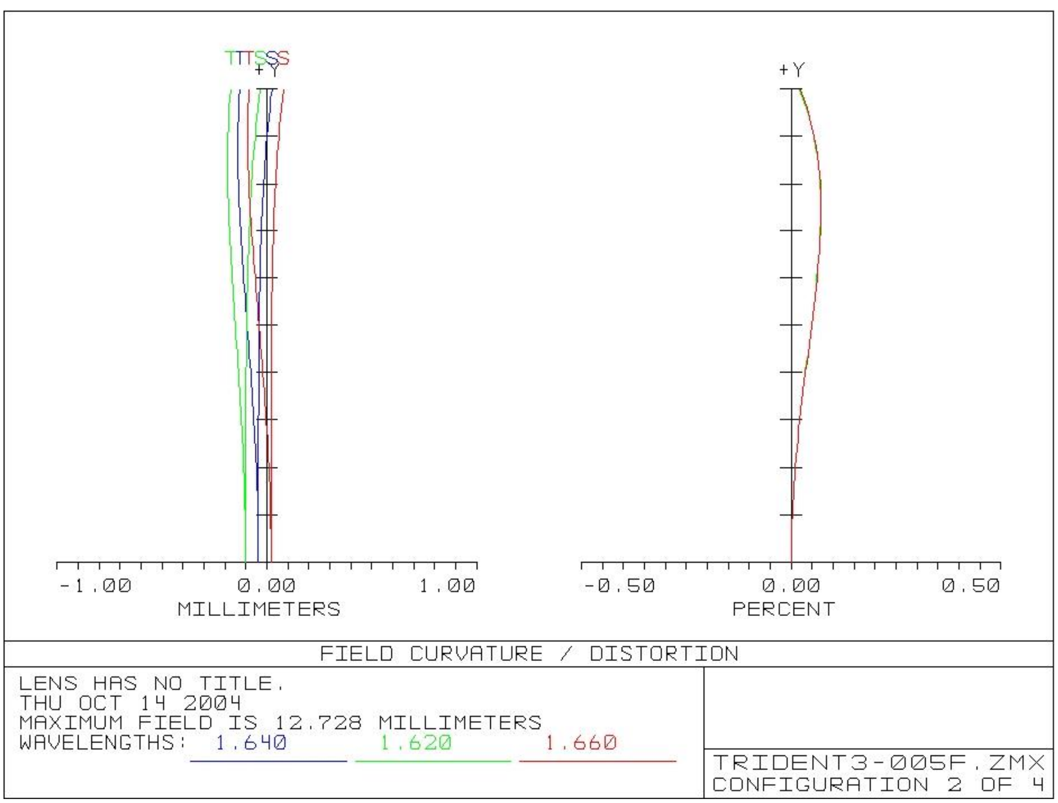

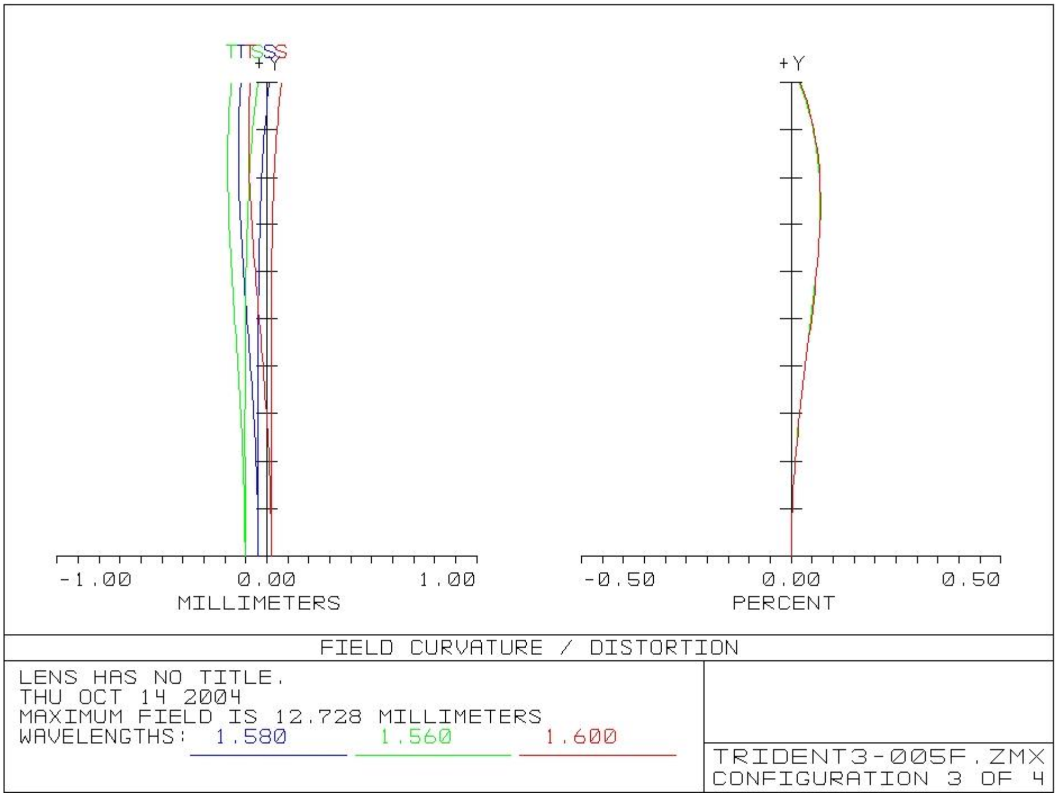
TTTSSS
+Y
+Y
-1.00
0.00
1.00
MILLIMETERS
-0.50
0.00
0.50
PERCENT
FIELD CURVATURE / DISTORTION
LENS HAS NO TITLE.
THU OCT 14 2004
MAXIMUM FIELD IS 12.728 MILLIMETERS
WAVELENGTHS: 1.580 1.560 1.600
TRIDENT3-005F.ZMX
CONFIGURATION 3 OF 4

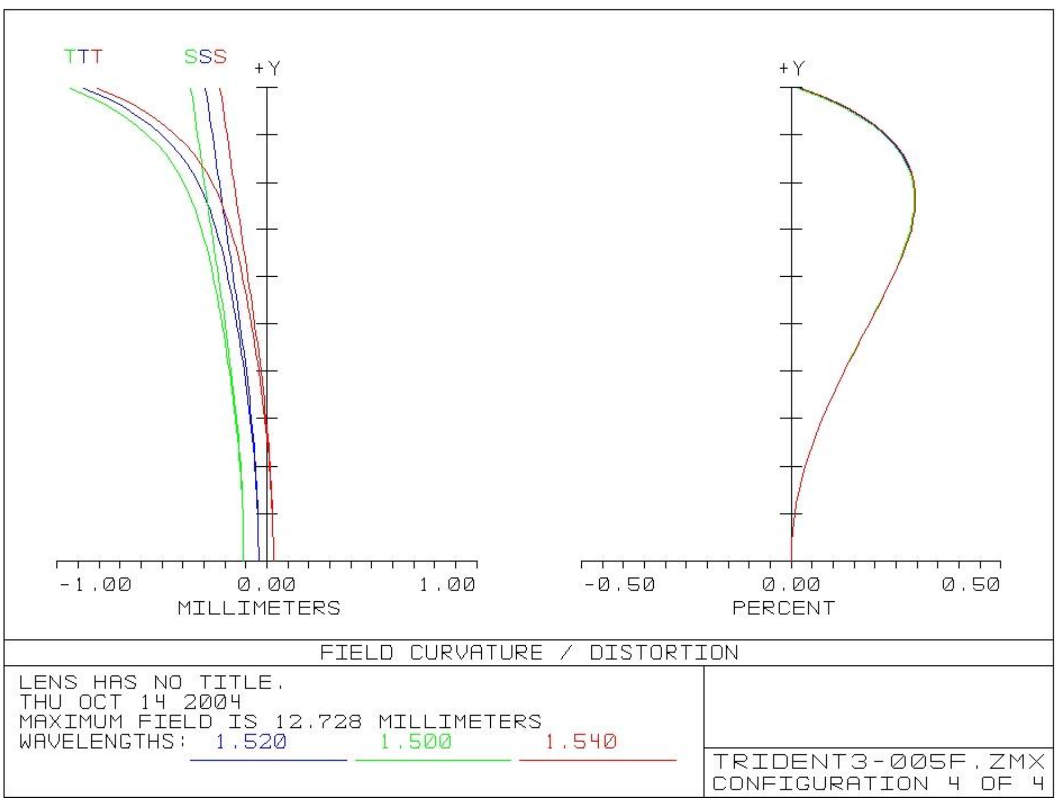
TTT
SSS
+Y
+Y
-1.00
0.00
1.00
MILLIMETERS
-0.50
0.00
0.50
PERCENT
FIELD CURVATURE / DISTORTION
LENS HAS NO TITLE.
THU OCT 14 2004
MAXIMUM FIELD IS 12.728 MILLIMETERS
WAVELENGTHS: 1.520 1.500 1.540
TRIDENT3-005F.ZMX
CONFIGURATION 4 OF 4

6.11.5 Aberrations

Following is the aberration in each channel of the nominal design, expressed as Zernike Polynomials. The RMS (to centroid) is the RMS after subtracting out both piston and tilt. The RMS (to centroid) is most physically significant and is generally what is meant by 'the RMS'. Although ZEMAX uses the term 'centroid' for brevity, the reference point is not the diffraction intensity centroid, but the reference point which minimizes the variance of the wavefront.

Channel 1
Wavelength : 1.7000 µm

Field :	0.00, 0.00 mm
Peak to Valley (to centroid) :	0.23370843 waves
RMS (to centroid) :	0.07184197 waves
Variance :	0.00516127 waves squared
Strehl Ratio (Est) :	0.81565917
RMS fit error :	0.00000000 waves
Maximum fit error :	0.00000000 waves

Piston	Z 1	0.12026415 :	1
Defocus	Z 4	0.12485233 :	(2p^2 - 1)
Sphericity	Z 9	-0.00322895 :	(6p^4 - 6p^2 + 1)
	Z 16	-0.00799308 :	(20p^6 - 30p^4 + 12p^2 - 1)

Field :	9.00, 9.00 mm
Peak to Valley (to centroid) :	0.64916769 waves
RMS (to centroid) :	0.12994903 waves
Variance :	0.01688675 waves squared
Strehl Ratio (Est) :	0.51341941
RMS fit error :	0.00001132 waves
Maximum fit error :	0.00007634 waves

Piston	Z 1	0.02715472 :	1
Tilt X	Z 2	-0.00079002 :	(p) * COS (A)
Tilt Y	Z 3	-0.00079002 :	(p) * SIN (A)
Defocus	Z 4	-0.00667819 :	(2p^2 - 1)
Astigmatism Y	Z 6	0.30198150 :	(p^2) * SIN (2A)
Coma X	Z 7	-0.04421086 :	(3p^2 - 2) p * COS (A)
Coma Y	Z 8	-0.04421086 :	(3p^2 - 2) p * SIN (A)
Sphericity	Z 9	-0.04243239 :	(6p^4 - 6p^2 + 1)
Astigmatism Trefoil X	Z 10	-0.05252620 :	(p^3) * COS (3A)
Astigmatism Trefoil Y	Z 11	0.05252620 :	(p^3) * SIN (3A)
Sphericity Astigmatism Y	Z 13	-0.03146052 :	(4p^2-3) p^2 * SIN (2A)
Quadratic Astigmatism X	Z 14	-0.02993909 :	(1Op^4 - 12p^2 + 3) p * COS (A)
Quadratic Astigmatism Y	Z 15	-0.02993909 :	(1Op^4 - 12p^2 + 3) p * SIN (A)
	Z 16	-0.00867776 :	(20p^6 - 30p^4 + 12p^2 - 1)
	Z 17	-0.00202948 :	(p^4) * COS (4A)

Channel 2
Wavelength : 1.6400 µm

Field :	0.00, 0.00 mm
Peak to Valley (to centroid) :	0.20865995 waves
RMS (to centroid) :	0.06475872 waves
Variance :	0.00419369 waves squared
Strehl Ratio (Est) :	0.84741876
RMS fit error :	0.00000000 waves
Maximum fit error :	0.00000000 waves

Piston	Z 1	0.09983779 :	1
Defocus	Z 4	0.11258467 :	(2p^2 - 1)
Sphericity	Z 9	0.00467764 :	(6p^4 - 6p^2 + 1)
	Z 16	-0.00824948 :	(20p^6 - 30p^4 + 12p^2 - 1)

Field :	9.00, 9.00 mm
Peak to Valley (to centroid) :	0.33477050 waves
RMS (to centroid) :	0.06709625 waves
Variance :	0.00450191 waves squared
Strehl Ratio (Est) :	0.83716996
RMS fit error :	0.00000785 waves
Maximum fit error :	0.00005367 waves

Piston	Z 1	0.04226631 :	1
Tilt X	Z 2	0.20258328 :	(p) * COS (A)
Tilt Y	Z 3	0.20258328 :	(p) * SIN (A)
Defocus	Z 4	0.00345776 :	(2p^2 - 1)
Astigmatism Y	Z 6	0.11291953 :	(p^2) * SIN (2A)
Coma X	Z 7	0.05612713 :	(3p^2 - 2) p * COS (A)
Coma Y	Z 8	0.05612713 :	(3p^2 - 2) p * SIN (A)
Sphericity	Z 9	-0.04788234 :	(6p^4 - 6p^2 + 1)
Astigmatism Trefoil X	Z 10	-0.05468999 :	(p^3) * COS (3A)
Astigmatism Trefoil Y	Z 11	0.05468999 :	(p^3) * SIN (3A)
Sphericity Astigmatism Y	Z 13	-0.04679829 :	(4p^2-3) p^2 * SIN (2A)
Quadratic Astigmatism X	Z 14	-0.03109059 :	(1Op^4 - 12p^2 + 3) p * COS (A)
Quadratic Astigmatism Y	Z 15	-0.03109059 :	(1Op^4 - 12p^2 + 3) p * SIN (A)
	Z 16	-0.00921752 :	(20p^6 - 30p^4 + 12p^2 - 1)
	Z 17	-0.00105126 :	(p^4) * COS (4A)

Channel 3
Wavelength : 1.5800 µm

Field :	0.00, 0.00 mm
Peak to Valley (to centroid) :	0.20940621 waves
RMS (to centroid) :	0.06515496 waves
Variance :	0.00424517 waves squared
Strehl Ratio (Est) :	0.84569834
RMS fit error :	0.00000000 waves
Maximum fit error :	0.00000000 waves

Piston	Z 1	0.10087105 :	1
Defocus	Z 4	0.11326512 :	(2p^2 - 1)
Sphericity	Z 9	0.00402445 :	(6p^4 - 6p^2 + 1)
	Z 16	-0.00855662 :	(20p^6 - 30p^4 + 12p^2 - 1)

Field :	9.00, 9.00 mm
Peak to Valley (to centroid) :	0.30143910 waves
RMS (to centroid) :	0.06111524 waves
Variance :	0.00373507 waves squared
Strehl Ratio (Est) :	0.86290150
RMS fit error :	0.00000777 waves
Maximum fit error :	0.00005297 waves

Piston	Z 1	0.04130277 :	1
Tilt X	Z 2	0.20666465 :	(p) * COS (A)
Tilt Y	Z 3	0.20666465 :	(p) * SIN (A)
Defocus	Z 4	-0.00011395 :	(2p^2 - 1)
Astigmatism Y	Z 6	0.08545073 :	(p^2) * SIN (2A)
Coma X	Z 7	0.05661252 :	(3p^2 - 2) p * COS (A)
Coma Y	Z 8	0.05661252 :	(3p^2 - 2) p * SIN (A)
Sphericity	Z 9	-0.05081274 :	(6p^4 - 6p^2 + 1)
Astigmatism Trefoil X	Z 10	-0.05631851 :	(p^3) * COS (3A)
Astigmatism Trefoil Y	Z 11	0.05631851 :	(p^3) * SIN (3A)
Sphericity Astigmatism Y	Z 13	-0.04893873 :	(4p^2-3) p^2 * SIN (2A)
Quadratic Astigmatism X	Z 14	-0.03216533 :	(1Op^4 - 12p^2 + 3) p * COS (A)
Quadratic Astigmatism Y	Z 15	-0.03216533 :	(1Op^4 - 12p^2 + 3) p * SIN (A)
	Z 16	-0.00954888 :	(20p^6 - 30p^4 + 12p^2 - 1)
	Z 17	-0.00100205 :	(p^4) * COS (4A)
	Z 22	-0.00100631 :	(15p^4 - 20p^2 + 6) p^2 * SIN (2A)

Channel 4

Wavelength : 1.5200 µm

Field :	0.00, 0.00 mm
Peak to Valley (to centroid) :	0.17124342 waves
RMS (to centroid) :	0.05474015 waves
Variance :	0.00299648 waves squared
Strehl Ratio (Est) :	0.88843265
RMS fit error :	0.00000000 waves
Maximum fit error :	0.00000000 waves

Piston	Z 1	0.09004700 :	1
Defocus	Z 4	0.09490377 :	(2p^2 - 1)
Sphericity	Z 9	-0.00422006 :	(6p^4 - 6p^2 + 1)
	Z 16	-0.00927619 :	(20p^6 - 30p^4 + 12p^2 - 1)

Field :	9.00, 9.00 mm
Peak to Valley (to centroid) :	1.15819517 waves
RMS (to centroid) :	0.28929684 waves
Variance :	0.08369266 waves squared
Strehl Ratio (Est) :	0.00000000
RMS fit error :	0.00064682 waves
Maximum fit error :	0.00360782 waves

Piston	Z 1	0.51277036 :	1
Tilt X	Z 2	0.32348217 :	(p) * COS (A)
Tilt Y	Z 3	0.32348217 :	(p) * SIN (A)
Defocus	Z 4	0.33675981 :	(2p^2 - 1)
Astigmatism Y	Z 6	0.42569245 :	(p^2) * SIN (2A)
Coma X	Z 7	0.15279089 :	(3p^2 - 2) p * COS (A)
Coma Y	Z 8	0.15279089 :	(3p^2 - 2) p * SIN (A)
Sphericity	Z 9	-0.18870245 :	(6p^4 - 6p^2 + 1)
Astigmatism Trefoil X	Z 10	0.01793550 :	(p^3) * COS (3A)
Astigmatism Trefoil Y	Z 11	-0.01793550 :	(p^3) * SIN (3A)
Sphericity Astigmatism Y	Z 13	-0.15403277 :	(4p^2-3) p^2 * SIN (2A)
Quadratic Astigmatism X	Z 14	-0.00700369 :	(1Op^4 - 12p^2 + 3) p * COS (A)
Quadratic Astigmatism Y	Z 15	-0.00700369 :	(1Op^4 - 12p^2 + 3) p * SIN (A)
	Z 16	-0.01300780 :	(20p^6 - 30p^4 + 12p^2 - 1)
	Z 17	-0.03396753 :	(p^4) * COS (4A)
	Z 22	-0.00285644 :	(15p^4 - 20p^2 + 6) p^2 * SIN (2A)
	Z 26	0.00670472 :	(p^5) * COS (5A)
	Z 27	0.00670472 :	(p^5) * SIN (5A)
	Z 28	-0.00194083 :	(6p^2 - 5) p^4 * COS (4A)

6.12 Error budget

6.12.1 Wavefront error

Based on the performance document (see XXX), the maximum WFE introduced by the imager optical system can be defined by the sensitivity of the ensquared energy to optical aberrations. As shown in the figure below, the ensquared energy depends on the aberration type and level. We also considered the wavefront error as a throughput additional loss because some light will be loss during the image integration process.

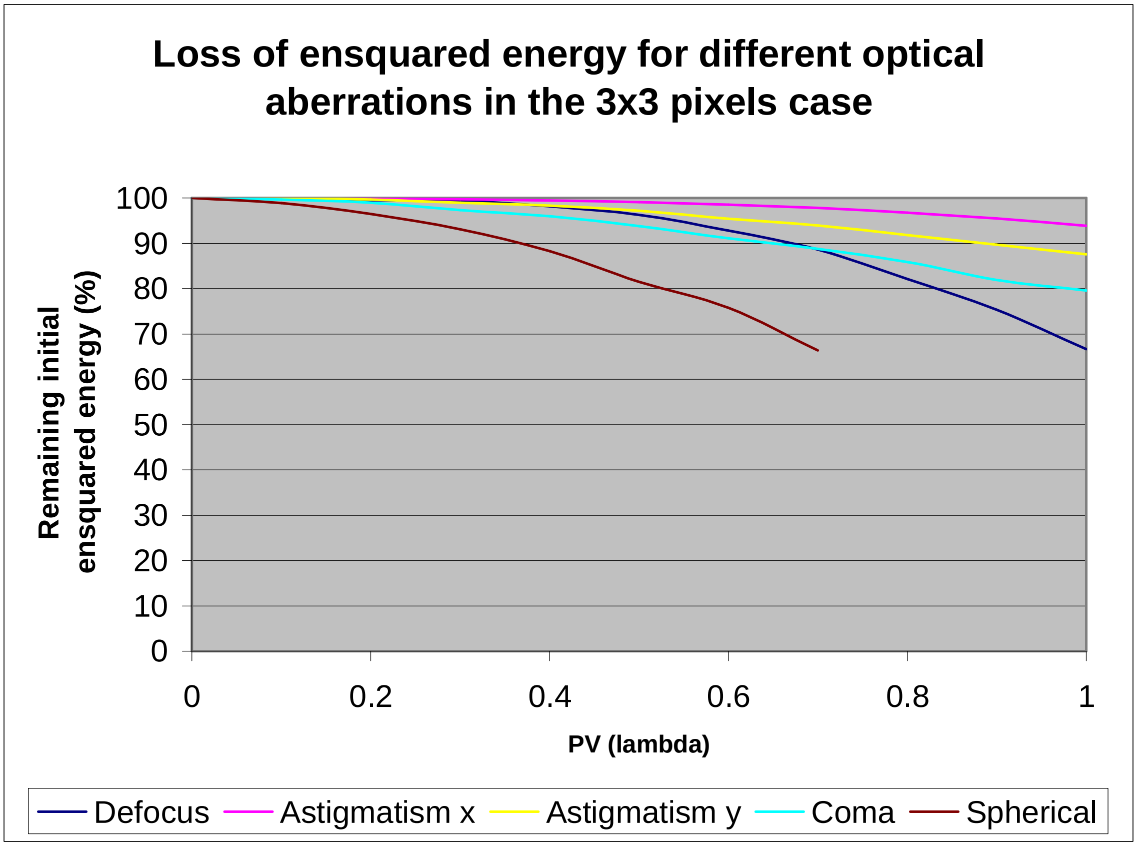

It is important to characterize the influence of the different optical aberrations on the camera performances in order to determine the optical design requirements. To do so, a Zernike fringe phase surface is applied to an image of a microlens, which is then refocused on the detector. In this setting, only one microlens is illuminated by a top hat function. The metric chosen is the ensquared energy. Though, the absolute value of the ensquared energy in a given square calculated by Zemax fluctuates with different sampling and is then not reliable. The metric will then be the relative variation of the ensquared energy of a given aberration compared to the case with no aberration for a constant sampling. It is considered that there is one guard pixel and that the PSF is centered in the middle of the remaining pixels. The aberrations investigated were defocus, astigmatism in x and in y, coma and spherical aberration.

It can be seen from the graphics that the ensquared energy is very sensible to spherical aberration. The maximal loss of ensquared energy per lenslet subaperture is set 10% in which case the optical system would need to have aberrations less than 0.3λ peak-to-valley at the design wavelength. This sets the limit for the optical system image quality.

6.12.2 Boresight or images registration error

The four independent images will be adjacent to each other. Differential error between images can be defined by three items: Magnification, distortion and boresight (image translation). All those three errors can be corrected by proper calibration. However we will maximize the pixel coverage of each images as well as the difference between each images.

During the tolerancing process, not only the WFE will be evaluated but also magnification, distortion and boresight.

At that time, no exact requirement is defined but a few pixels should be acceptable.

6.12.3 Field position error

The non-uniform WFE along the field of view will affect the imager performance by producing artificial vignetting of the signal, which can affect the instrument behaviors. Uniformity of the performance along the FOV is important.

At that time, no exact requirement is defined but less than 5% variation should be acceptable.

6.12.4 Wavefront error budget

The total wavefront error (WFE) is made up of in

6.12.5 Design tolerance

The most realistic way to predict the performance of an optical system with a set of optical and mechanical tolerances is to do a Monte Carlo analysis that includes all the tolerances of the system. This simulates the simultaneous effect of all the perturbations. The result of the Monte Carlo analysis is the probability that a single system will meet the required specification. However, the approach proposed for MWI will be different and could be qualified of more pessimistic. It is actually the most widely used approach in optical tolerancing, which consists in separating the fabrication and alignment tolerance analyses. For each of these, a Monte Carlo analysis is done, which yields the expected change in a characteristic for a given set of tolerances. The value of the change is such that 90% of the systems simulated show a change lower than this value. The optical system is said to meet the specified requirements when the sum of the changes caused exclusively by fabrication, alignment and environmental variations is smaller than about 90% of the maximum acceptable change of the characteristic. This leaves a margin of 10% for unpredictable perturbations. Of course, an analysis including all the tolerances simultaneously is desirable in order to make sure that the predicted change in a characteristic does not exceed the one obtained using the more pessimistic scenario, which rarely happens.

Global tolerance budget. (TBC)

Characteristic	Nominal Value	Effect of fabrication errors	Effect of alignment errors	Desirable maximum change caused by environment variations	~10% margin	Required maximum change
RMS wavefront aberration. (λ = 0.633 µm)						
RMS spot size on the detector (µm)						
Mag. changes						
Distortion						
Position on the detector (µm)						

Manufacturer of optical components uses general tolerance specifications to provide guideline for manufacturing capabilities. We know that those limits are not absolute and tighter tolerances may be possible but using such manufacturing tolerances will be safer approach.

In general, optics manufacturing tolerances can be divided into commercial quality, precision quality and manufacturing limits.

Optical component drawing will be prepared using the ISO 10110 standard.

6.12.5.1 Surface irregularities

The surface irregularities of all optical components use in the MWI will have a maximum of 0.5 fringe at 633 nm.

The requirement is applied to transmission surfaces but also to reflective surfaces.

6.12.5.2 Component fabrication errors

Most of the optical components such as lenses, windows and mirror will use the following manufacturing tolerances:

Attribute/when applicable	Quality	Comments
Glass Quality index V-number	 +/-0.001 +/-0.5%	 Commercial grade Margin for cryogenic index uncertainties
Diameter (mm)	+0.00,	Precision grade

	-0.025	
Center Thickness (mm)	+/-0.050	
Sag (mm)	+/-0.025	
Radius	+/-0.1%	Can be relaxed for some component
Irregularity (fringe)	0.5	
Wedge Lens (ETD, mm)	0.01	
Wedge Prim (TIA, arcmin)	+/-0.5	
Scratch-Dig	60-40	
Surface Roughness (nm RMS)	<2nm	
AR coating (R_{ave})	<0.5%	Possible for a limited bandpass between 1.5 and 1.8 um.

6.12.5.3 Alignment errors

Alignment errors is mainly the positioning error consisting of the lateral and axial position error as well as the wedge error.

6.12.5.4 Refractive index Errors

6.13 Ghost images

Ghost images are formed by an even number of spurious reflections from optical surfaces. The surface reflectivity is small (less than 0.5%), and so those ghosts produced by double reflections tend to dominate. The most important tend to involve a first reflection from the detector because it has high reflectivity (about 20%).

The complex structure of the MW-splitter produces also strong ghost due to multiple reflection. Proper study of ghost produces by MW-splitter will be done using non-sequential ray tracing and/or ASAP software.

6.13.1 Filter Ghost

6.13.2 Detector Ghost

6.13.3 Cryostat Window Ghost

6.13.4 Other Ghost

6.14 Lens Mounting System

6.15 Cryogenic Compensation

6.16 Filter Selection

6.17 Throughput

The lenses will be coated with standard A/R coatings, with less than 0.5% reflectivity for a waveband between 1.50 and 1.72µm.

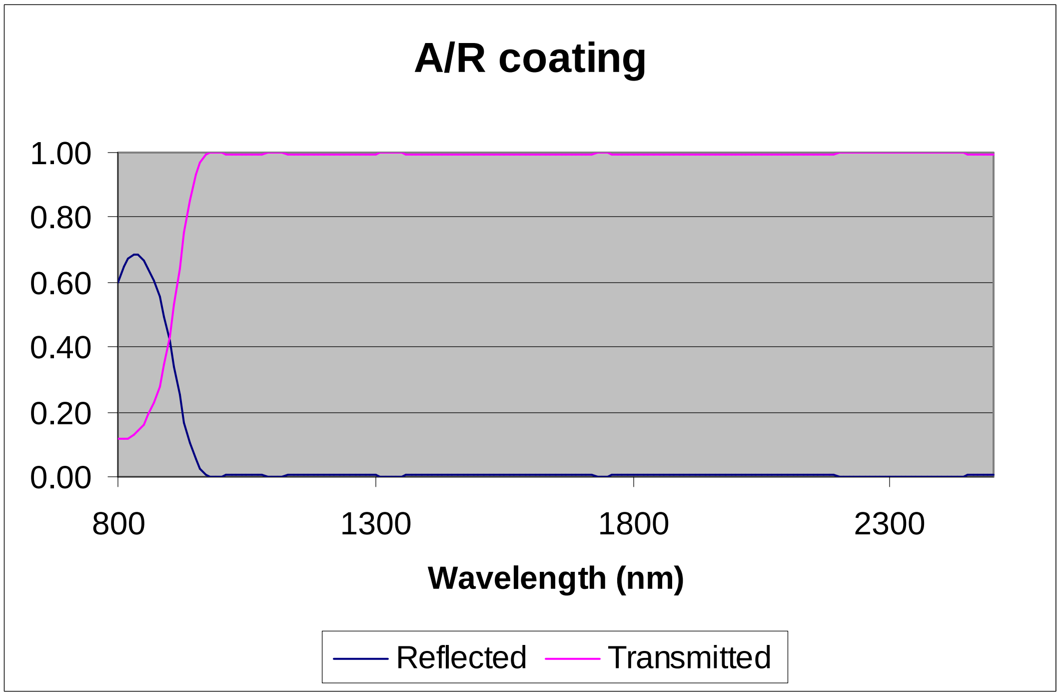

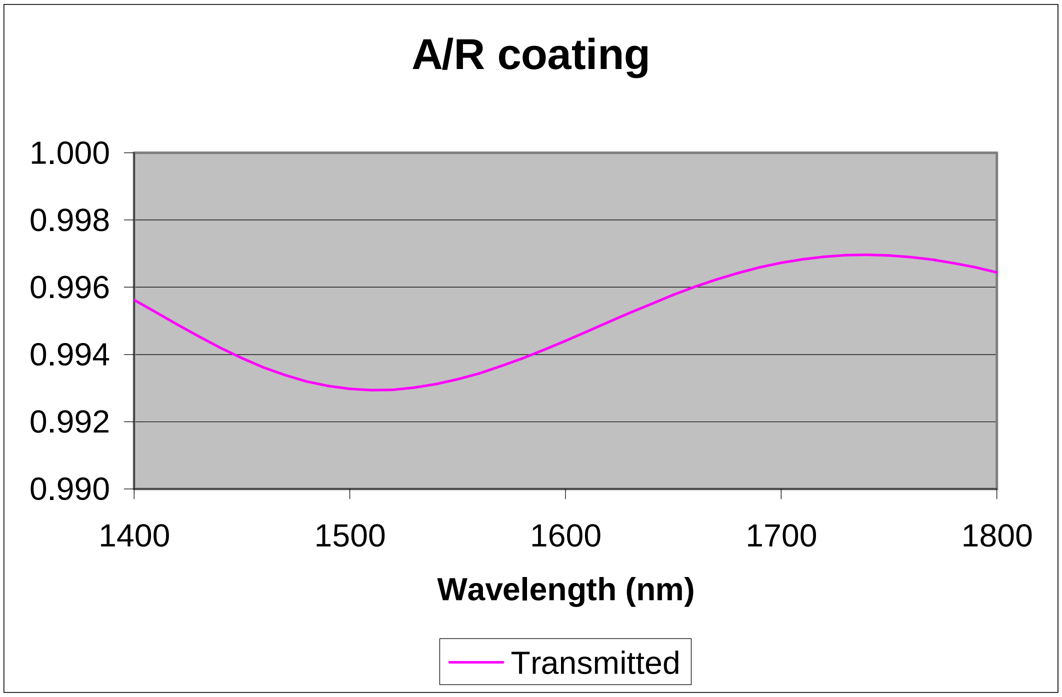

Considering the coatings, the number of surfaces and the absorption of materials used, but not considering the dichroic splitting surfaces inside the MW-splitter cube, we will have a maximum transmission between 83% (channel 4) and 88% (channel 1).

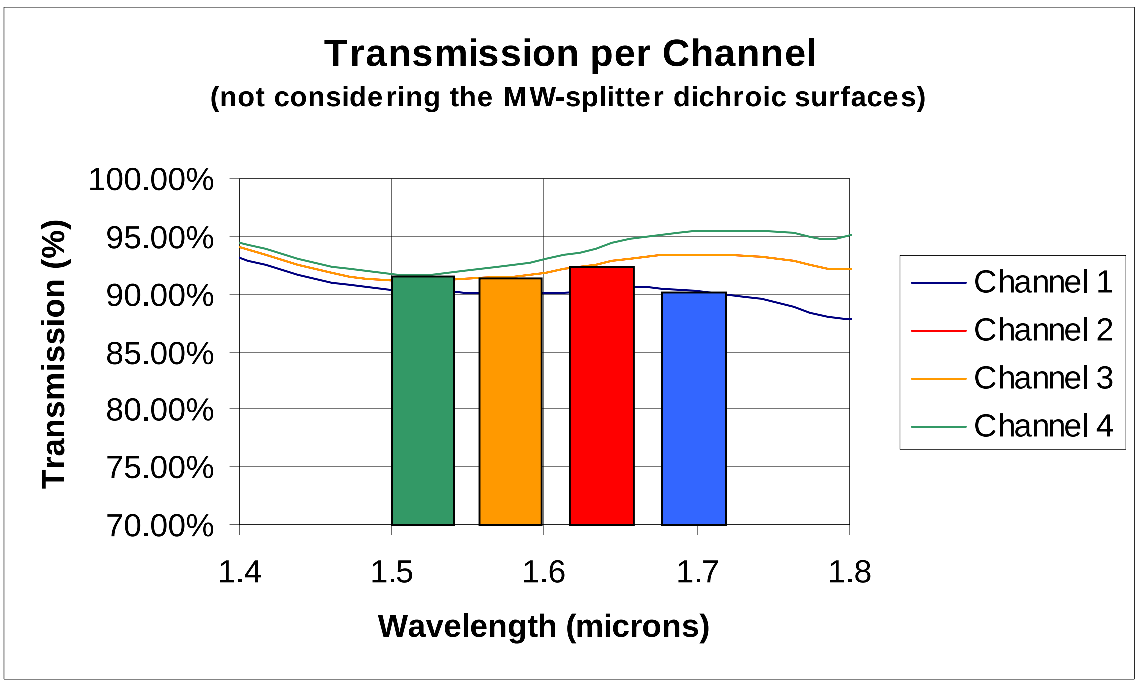

We will have to add the transmission of the various spectral filters through the MW-splitter cube. Assuming that each dichroic filter has a transmission of approximately

90%, we will have a peak transmission between 90% and 95% per channel. We should expect a fabrication error of 0.1-0.2% on transmission ratio for each coated surface.

6.18 Cold Stop Performance

Cold stop performance is mainly related to the imaging quality of the coronagraph output OAP. This will be addressed in the EXAOC projects.

No pupil viewing mode is implemented

6.19 Emissivity

The MWI design meets the requirement of an effective instrument emissivity of < 1% at wavelength > 2um and an instrument photon background less than one half of the detector dark current.

The cryostat window is the dominant contributor to the instrument effective emissivity. In the near infrared, the absorption coefficient of IR-grade fused silica is about $1X10^{-5}$ cm^{-1}. This window should have a 10 mm thickness with an emissivity of 0.00001. Assuming that the contribution from other components in the cryostat is small, the instrument effective emissivity is less than 0.001%. This window requires a cleaning procedure to prevent dust and additional emissivity.

6.20 Baffling

The nature of the EXAOC offers a natural baffling scheme due to the partitioning of the instrument into many zones. Many apertures will offer also natural baffles. Analysis of the baffles must be undertaken for the MWI using both Zemax (Non-sequential) and ASAP (from Breault Research Organization) softwares.

6.21 Blackening

Special paint INO

6.22 Thermal Radiation

The imager chamber is a close cavity held at a constant temperature. Based on black body radiation, we will calculate a safer cryostat temperature. Experience has shown that 150K is enough to ensure that radiation flux below the detector dark current. No problem is expected from the thermal radiation.

6.23 Lens Manufacturing and delivery delay

TBD

6.24 Optical Design Risks

6.24.1 Input from coronagraph

The baseline design for the MWI system is based on a coronagraph input beam which is defined by EXAOC level requirements. Any modification in this input from the coronagraph may have an impact of the MWI system design.

6.24.2 Lens Manufacture

Special form requirement for the lenses may affect the cost and procurement of those lenses. Manufacturing test must be conducted to identify potential problems. Particular discussion with supplier will be required in order to fulfill the optical requirement.

6.24.3 MW-splitter Assembly

The particular assembly requirements should be considered as potential risk. Assembly test under cryogenic environment must be undertaken earlier in the project including optical cement adhesion and transmission test under vacuum and cryogenic temperature.

Design variant using thin parallel plate dichroic will be design and evaluated at the critical design phase.

6.24.4 Dichroic and bandpass filter Design

Thin film requirement on for the combination of dichroic and bandpass filter must be considered as a risky item. Manufacturing difficulty and cost should have a significant impact on the project. Commencing purchase negotiations as soon as possible would minimize delays.

Bandpass filter width versus dichroic slope study must be done at the critical design phase to identify the best way to achieve acceptable transmission, rejection and performance level. Some science objectives may be unachievable if the performance is inadequate.

6.25 Cryostat Window location

TBD